FACULDADE DE ENGENHARIA DA UNIVERSIDADE DO PORTO

Gateway Positioning in Flying Networks

Hugo Daniel Teixeira Rodrigues

Mestrado Integrado em Engenharia Eletrotécnica e de Computadores

Supervisor: Dr. Rui Lopes Campos

Co-Supervisor: Eng. André Filipe Coelho

July 30, 2020

Abstract

Over the past few years, the usage of Unmanned Aerial Vehicles (UAVs) for a myriad of applications, both civil and military, has increased. As UAVs are able to operate virtually anywhere, hover above the ground, and carry cargo, they constitute perfect platforms for transporting communications nodes on board, including Wi-Fi Access Points and cellular Base Stations.

In this sense, there has been an increasing interest in using UAVs to deploy Flying Networks (FNs), which constitute an agile and flexible solution to establish communications networks and reinforce telecommunications infrastructures on demand, enabling the broadband Internet access in temporary events. However, FNs impose significant challenges regarding the positioning of the UAVs. In the literature, some solutions have been proposed for the positioning of the UAVs that act as Flying Access Points (FAPs); yet, the positioning of the Gateway (GW) UAV has been overlooked. An additional problem when deploying FNs is the total amount of time that UAVs can remain operational, as they have batteries with limited capacity, whose energy can be drained fast.

As the overall network performance can be improved if the GW UAV remains operational for the maximum amount of time, since it is the communications node in charge of connecting the FN to the Internet, the development of an energy-aware GW UAV positioning solution that minimizes the UAV energy consumption without compromising the Quality of Service (QoS) provided is the scope dissertation.

The main contributions of this dissertation are two-fold: 1) the Energy-aware GateWay Positioning (EGWP) algorithm, which defines the trajectory and speed of the GW UAV that minimizes its energy consumption, without compromising the QoS, and taking into account the traffic demands of the FAPs; and 2) a UAV power consumption simulator, called UAVPowerSim, that can be used to evaluate the power consumption and lifetime of a UAV moving along a trajectory.

UAVPowerSim was used to validate and evaluate the EGWP algorithm, allowing to conclude about the gains achieved in energy consumption and lifetime of the GW UAV. Moreover, the network performance when the EGWP algorithm is employed was evaluated by means of ns-3 simulations. The evaluation results show gains up to 16% in energy consumption for a degradation lower than 1% in aggregate throughput and an increase of 16% in delay, considering as baseline the GW UAV hovering in the optimal position defined by a state of the art GW UAV positioning algorithm.

Resumo

Nos últimos anos, o uso de Veículos Aéreos Não Tripulados (UAVs) para uma infinidade de aplicações, civis e militares, aumentou. Como os UAVs são capazes de operar virtualmente em qualquer lugar, pairar sobre o solo e transportar carga, eles constituem plataformas perfeitas para o transporte de nós de comunicações a bordo, incluindo Pontos de Acesso Wi-Fi e Estações Base celulares.

Neste sentido, tem havido um interesse crescente no uso de UAVs para implantar Redes Voadoras (FNs), que constituem uma solução ágil e flexível para estabelecer redes de comunicações e reforçar as infraestruturas de telecomunicações existentes mediante a procura, permitindo o acesso à Internet de banda larga em eventos temporários. No entanto, as FNs impõem desafios significativos em relação ao posicionamento dos UAVs. Na literatura, algumas soluções foram propostas para o posicionamento dos UAVs que atuam como Pontos de Acesso Voadores (FAPs); contudo, o posicionamento do *gateway* (GW) UAV não foi estudado com a profundidade suficiente. Um problema adicional que surge ao implantar FNs é a quantidade total de tempo que os UAVs podem permanecer operacionais, pois possuem baterias com capacidade limitada, cuja energia pode ser rapidamente consumida.

Como o desempenho global da rede pode ser melhorado se o GW UAV permanecer operacional pela quantidade máxima de tempo possível, uma vez que é o nó de comunicações responsável por ligar a FN à Internet, o desenvolvimento de uma solução de posicionamento do GW UAV com consicência energética, que minimize o consumo de energia sem comprometer a Qualidade de Serviço (QoS) oferecida, é o foco desta dissertação.

As principais contribuições desta dissertação são duas: 1) o algoritmo *Energy-aware GateWay Positioning* (EGWP), que define a trajetória e a velocidade do GW UAV que minimiza o seu consumo energético, sem comprometer a QoS oferecida, tendo em conta as necessidades de tráfego dos FAPs; e 2) um simulador do consumo de energia de UAV, chamado UAVPowerSim, capaz de avaliar o consumo e o tempo de vida de um UAV que se move ao longo de uma trajetória.

O UAVPowerSim foi utilizado para validar a avaliar o algoritmo EGWP, permitindo tirar conclusões sobre os ganhos no consumo de energia e no tempo de vida do GW UAV. Além disso, o desempenho em termos de QoS da rede quando o algoritmo EGWP é empregue foi avaliado por meio de simulações ns-3. A avaliação do algoritmo EGWP, realizada em vários cenários de rede, incluindo diferentes números de FAPs e diferentes distâncias médias entre eles, permitiu concluir ganhos até 16% no consumo de energia, para uma degradação inferior a 1% em débito binário agregado e um aumento de 16% em atraso, considerando como linha de base o GW UAV a pairar na posição ótima definida por um algoritmo do estado da arte.

Acknowledgments

First, I would like to express my gratitude to my supervisors, Dr. Rui Campos, and Eng. André Coelho, for all the support during this dissertation, and the ongoing availability to answer my questions and doubts.

To my friends, thank you for always being there for me, for believing in me even when I don't believe in myself.

To my family, all my gratitude for always supporting my dreams and making me the person I am today.

This work is co-financed by the ERDF – European Regional Development Fund through the Operational Programme for Competitiveness and Internationalisation - COMPETE 2020 and the Lisboa2020 under the PORTUGAL 2020 Partnership Agreement, and through the Portuguese National Innovation Agency (ANI) as a part of the projects «CHIC: POCI-01-0247-FEDER-024498» and «5G: POCI-01-0247-FEDER-024539».

Hugo Rodrigues

“Freedom is the freedom to say that two plus two make four.
If that is granted, all else follows.”

George Orwell

Contents

1 Introduction **1**
1.1 Context . . . 1
1.2 Motivation and Problem . . . 2
1.3 Objectives . . . 3
1.4 Contributions . . . 3
1.5 Document Structure . . . 3

2 State of the Art **5**
2.1 Introduction . . . 5
2.2 Flying Networks . . . 5
2.2.1 Controlled Mobility of the Communications Nodes . . . 6
2.2.2 UAV Positioning . . . 6
2.2.3 Energy in Flying Networks . . . 8
2.3 Gateway Positioning . . . 12
2.3.1 Wireless Mesh Networks . . . 12
2.3.2 Flying Networks . . . 16
2.4 Summary and Main Conclusions . . . 17

3 Energy-aware Gateway Positioning Algorithm **19**
3.1 System Model and Problem Formulation . . . 19
3.2 Energy-aware Gateway Positioning algorithm . . . 23
3.3 Summary . . . 27

4 UAV Power Simulator **29**
4.1 UAV Power Simulator Input Parameters . . . 29
4.2 UAV Power Simulator Implementation . . . 31
4.3 UAV Power Simulator Output . . . 35
4.4 Summary . . . 35

5 Solution Evaluation **37**
5.1 Evaluation Conditions . . . 37
5.2 Energy Consumption and Network Performance Evaluation . . . 37
5.2.1 ns-3 Simulation Setup . . . 38
5.2.2 Evaluation Under Typical Networking Scenarios . . . 39
5.2.3 Evaluation Under Random Networking Scenarios . . . 51
5.3 Discussion . . . 52

6 Conclusions **55**

References 57

List of Figures

1.1 Flying Network deployed in a festival providing Internet connectivity to the users on the ground [3]. 2

2.1 Communications link rate range for two IEEE 802.11b nodes [8]. 7
2.2 Rotary Wing: Flying Speed vs. UAV Power Consumption [6][9]. 8
2.3 Rotary-Wing: Results obtained through real-world tests [10]. 9
2.4 Fixed Wing: Flying Speed vs UAV Power Consumption [9]. 10
2.5 Required Power for Hovering vs. Payload Weight [12]. 11
2.6 Evaluation by Channel-Radio Association. 13
2.7 Evaluation by Optimization Techniques. 13
2.8 Evaluation by Architecture. 14
2.9 Evaluation of network performance metrics. 14
2.10 Simple scenario used to evaluate the GWP algorithm [4]. 16
2.11 Complex scenario used to evaluate the GWP algorithm [4]. 17

3.1 System Elements. 20
3.2 MCS index information for the IEEE 802.11ac technology [19]. 21
3.3 Propulsion power consumption versus UAV speed V [6]. 22
3.4 Reference scenario. 22
3.5 Spheres representing the communications range of each FAP, considering the FSPL model, constrained by the SNR value that enables the selection of an MCS index compliant with the traffic demand. The intersection area, within which the GW UAV can move, results from the intersection of the spheres. 25
3.6 Trajectory examples. 25

4.1 Communications range for each FAP and the resulting volume of the intersection. 32
4.2 Different intersections between two FAPs. 33
4.3 Trajectory examples. 33
4.4 Selected trajectory, which is the one with the greatest distance, thus allowing to minimize the power consumption. 34
4.5 Graphical results provided by UAVPowerSim for energy consumption. 35
4.6 Graphical results provided by UAVPowerSim for operational time. 36
4.7 UAVPowerSim terminal output. 36

5.1 Reference scenario. 38
5.2 Energy consumption results for 2 FAPs positioned close to each other. 40
5.3 Network performance results, considering the FSPL model, for 2 FAPs positioned close to each other. 40

5.4 Network performance results, considering the Rician fast-fading component, for 2 FAPs positioned close to each other. 40
5.5 Energy consumption results for 2 FAPs positioned at a considerable distance from each other. 41
5.6 Network performance results, considering the FSPL model, for 2 FAPs positioned at a considerable distance from each other. 42
5.7 Network performance results, considering the Rician fast-fading component, for 2 FAPs positioned at a considerable distance from each other. 42
5.8 Performance results considering the EGWP with and without SNR margin, complemented with results for hovering, for 2 FAPs positioned at a considerable distance from each other. 42
5.9 Energy consumption results for 2 FAPs positioned at a great distance from each other. 43
5.10 Network performance results, considering the FSPL model, for 2 FAPs positioned at a great distance from each other. 43
5.11 Network performance results, considering the Rician fast-fading component, for 2 FAPs positioned at a great distance from each other. 44
5.12 Energy consumption results for 5 FAPs positioned close to each other. 44
5.13 Network performance results, considering the FSPL model, for 5 FAPs positioned close to each other. 45
5.14 Network performance results, considering the Rician fast-fading component, for 5 FAPs positioned close to each other. 45
5.15 Energy consumption results for 5 FAPs positioned at a considerable distance from each other. 46
5.16 Network performance results, considering the FSPL model, for 5 FAPs positioned at a considerable distance from each other. 46
5.17 Network performance results, considering the Rician fast-fading component, for 5 FAPs positioned at a considerable distance from each other. 46
5.18 Energy consumption results for 5 FAPs positioned at a great distance from each other. 47
5.19 Network performance results, considering the FSPL model, for 5 FAPs positioned at a great distance from each other. 47
5.20 Network performance results, considering the Rician fast-fading component, for 5 FAPs positioned at a great distance from each other. 48
5.21 Energy consumption results for 10 FAPs positioned close to each other. 48
5.22 Network performance results, considering the FSPL model, for 10 FAPs positioned close to each other. 49
5.23 Network performance results, considering the Rician fast-fading component, for 10 FAPs positioned close to each other. 49
5.24 Energy consumption results for 10 FAPs positioned at a considerable distance from each other. 50
5.25 Network performance results, considering the FSPL model, for 10 FAPs positioned at a considerable distance from each other. 50
5.26 Network performance results, considering the FSPL model, for 10 FAPs positioned at a considerable distance from each other. 50
5.27 Network performance results considering the FSPL model, for 10 FAPs positioned at a great distance from each other. 51

5.28 Network performance results, considering the FSPL model, for 10 FAPs positioned at a great distance from each other. 51
5.29 Network performance results, considering the Rician fast-fading component, for 10 FAPs positioned at a great distance from each other. 52
5.30 Impact of both the average distance between the FAPs and the number of FAPs on the gains in the GW UAV lifetime obtained. 52

List of Tables

4.1 UAV and environment attributes [6]. 30

Acronyms and Abbreviations

AP	Access Point
CMMC	Capacity Maximization and Communication
CS	Central Station
CSMA/CA	Carrier Sense Multiple Access with Collision Avoidance
EEMC	Energy-Efficient Maneuvering and Communication
EGWP	Energy-aware Gateway Positioning
FAP	Flying Access Point
FN	Flying Network
FSLP	Free-space Path Loss
GDTSP	Greedy Dominating Tree Set Partitioning
GW	Gateway
GWP	GW UAV Placement
LoS	Line of Sight
MAC	Medium Access Control
MR	Mesh Router
MRMC	Multi-Radio Multi-Channel
PDR	Packet Delivery Ratio
PF	Potential Fields
PMMC	Power Minimization Maneuvering and Communication
QoS	Quality of Service
SINR	Signal-to-Interference-plus-Noise Ratio
SMS	Split-Merge-Shift
SNR	Signal-to-Noise Ratio
SRMC	Single-Radio Multi-Channel
SRSC	Single-Radio Single-Channel
TCE	Temporary Crowded Event
UAMA	User-Aware Approach with a Minimum Altitude Assignment
UARA	User-Aware Approach with a Random Altitude Assignment
UAV	Unmanned Aerial Vehicles
WMN	Wireless Mesh Networks

Chapter 1

Introduction

1.1 Context

In recent years there has been an increase in the usage of Unmanned Aerial Vehicles (UAVs) for a myriad of applications, both civil and military. Their capability to operate almost everywhere, their ability to hover above the ground, and their increasing capacity to carry cargo make UAVs perfect platforms for transporting communications nodes on board, including Wi-Fi Access Points and cellular Base Stations. This reality has prompted the interest in deploying Flying Networks (FNs) to establish and reinforce communications, and enable broadband Internet access in temporary events, including music festivals (Figure 1.1) and disaster scenarios. However, FNs impose important challenges regarding the positioning of the UAVs, in order to meet the Quality of Service (QoS) expected by the users. In this dissertation, we assume that two types of UAVs compose the FN: Flying Access Points (FAPs) and a single gateway (GW) UAV. In the literature, some solutions have been proposed for the positioning of FAPs, in order to enhance the radio coverage and the number of ground users served; a reference example is the NetPlan algorithm [1]. However, the positioning of the GW UAV has been overlooked. The GW UAV plays a crucial role in the FN, as it is the communications node responsible for forwarding the traffic between the FAPs and the Internet.

Another relevant aspect in the context of FNs is the UAVs lifetime. As the UAVs are not connected to the electrical grid, they rely on their onboard energy, thus limiting the FN endurance [2]. The problem is exacerbated if the UAV plays the role of GW UAV, especially in an FN composed of a single GW. The available energy at the GW UAV directly affects the QoS of the overall network since if the GW UAV becomes unavailable due to power shortage, the rest of the network will be unable to access the Internet.

With all that has been presented, the development of an energy-aware GW UAV positioning solution for FNs is the scope of this dissertation.

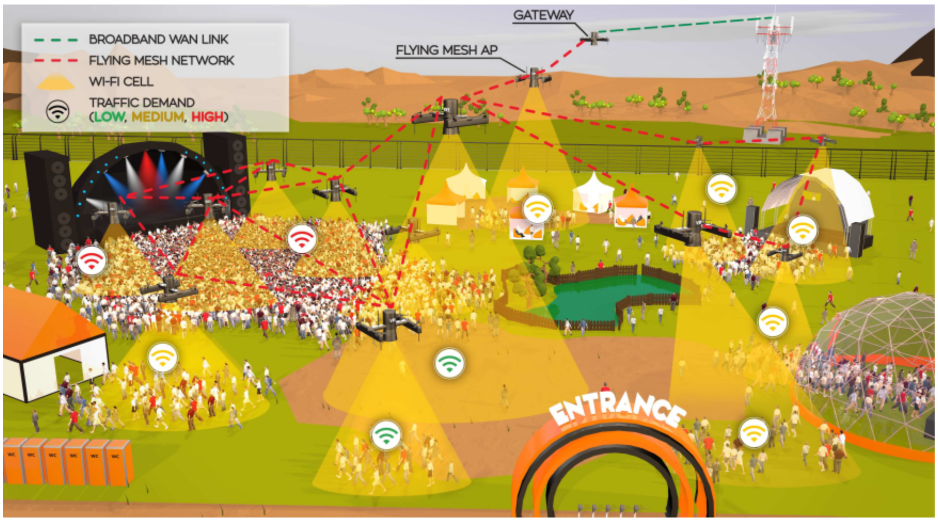

Figure 1.1: Flying Network deployed in a festival providing Internet connectivity to the users on the ground [3].

1.2 Motivation and Problem

Recently, a centralized routing solution for FNs, called RedeFINE, able to select high-capacity communications paths between UAVs while avoiding communications disruptions, by defining in advance the forwarding tables and the instants they shall be updated in the UAVs, was proposed in [3]. In RedeFINE, the forwarding decisions are performed by a Central Station (CS), which is also responsible for defining the positions of the UAVs acting as FAPs by running a state of the art FAPs positioning algorithm, thus providing a holistic knowledge of the network. However, RedeFINE was only evaluated in FNs without the capability to control the position of the GW UAV, which is the communications node responsible for forwarding the traffic between the FN and the Internet. In order to address this issue, a traffic-aware gateway positioning algorithm (GWP) for FNs with controlled topology was proposed in [4]. GWP considers the amount of traffic generated by the FAPs and their positions to define in advance the position of the GW UAV, taking advantage of the holistic knowledge provided by the CS. However, GWP neglects an important aspect: the energy consumption of the GW UAV.

Unlike ground-based networks, when planning FNs, we should take into consideration the UAVs battery capacity since it directly influences the total amount of time that the network is available. A longer lasting FN will be able to provide connectivity for a longer time, thus increasing the amount of traffic that can be exchanged. This problem is presented in [5], which identifies resource management and energy efficiency as open research challenges for the usage of UAVs in wireless networks. In the literature, the GW UAV positioning challenge has mainly been overlooked, to the best of our knowledge, as well as the issue of energy-efficient positioning of UAVs; the majority of the work has been focused on UAVs' trajectory optimization [6] [7].

For these reasons, a GW UAV positioning solution that meets the FAPs' traffic demands while ensuring an energy-aware UAV behavior is worth to be considered, in order to enable a longer-lasting FN and improve the QoS offered.

1.3 Objectives

In order to address the challenges that were previously stated, this dissertation presents as its main objective the development of an energy-aware GW UAV positioning solution that aims at maximizing the FN endurance, without compromising the QoS offered by the FN. As such, it envisions the following specific objectives:

- Development of an algorithm to determine the optimal positioning of the GW UAV, taking into account the traffic demand of the FAPs while reducing the energy consumption of the GW UAV. For that purpose, the challenges inherent in accomodating variable traffic demands, as well as the impact of both the trajectory and speed of the GW UAV are addressed.
- Development of a simulator to evaluate the energy consumption of the GW UAV.
- Validation and evaluation of the network performance using the ns-3 simulator, when the algorithm proposed by this dissertation is employed.

1.4 Contributions

The main contributions of this dissertation are two-fold:

- An Energy-aware GateWay Positioning (EGWP) algorithm for FNs with controlled topology. EGWP takes into consideration the energy consumed by the different movements of the UAV to define both the trajectory and speed of the GW UAV that minimizes its energy consumption, without compromising the QoS offered by the FN.
- A custom-tailored simulator, called UAVPowerSim, which was developed to evaluate the energy consumption of a UAV while in movement.

A journal paper about the EGWP algorithm has been submitted to IEEE Networking Letters.

1.5 Document Structure

The rest of this document is structured as follows:

- Chapter 2 [State of the Art] - Presentation of fundamental concepts and review of existing solutions that were considered to accomplish the objectives of this dissertation.
- Chapter 3 [Energy-aware Gateway Positioning Algorithm] - Definition of the problem statement and description in detail of the algorithm proposed in this dissertation.

- Chapter 4 [UAV Power Simulator] - Presentation of the simulator developed to evaluate the algorithm proposed in this dissertation.
- Chapter 5 [Solution Evaluation] - Validation and evaluation of the proposed algorithm in terms of energy consumption and network performance against the baseline, under different networking scenarios, and presentation and discussion of the results.
- Chapter 6 [Conclusions] - Conclusion of the dissertation, including the work done, main results achieved, and future work.

Chapter 2

State of the Art

2.1 Introduction

In this chapter, the fundamental concepts and existing solutions relevant to achieve the objectives presented in Chapter 1 are presented. Chapter 2 has the following structure.

- In Section 2.2, a brief introduction to FNs and fundamental concepts to the problem of this dissertation are presented, including:
  - Controlled Mobility of the Communications Nodes: how the position of the UAVs can be controlled.
  - UAV Positioning: how to address the UAV positioning challenge to enhance the network performance.
  - Energy in Flying Networks: how different types of UAV movements influence the energy consumption in UAVs.
- In Section 2.3, existing solutions for GW positioning in Wireless Mesh Networks and FNs are reviewed.
- Section 2.4, the summary of the state of the art reviewed and the main conclusions achieved are presented.

2.2 Flying Networks

With the need to provide Internet access in areas and situations where terrestrial networks are not the best option, several options began being studied, one of them being FNs. FNs present some advantages in a myriad of scenarios, as they can be quickly deployed on-demand anywhere, anytime. In FNs, the aerial links are characterized by a strong Line-of-Sight (LOS) component, which allows to use simplified radio propagation models for their planning, including the Free-space Path Loss (FSPL) model. UAVs have fully controllable mobility in 3D airspace and can adaptively change their locations for reducing distances with ground users, in order to improve the radio coverage and QoS offered. These advantages gained relevance thanks to the advent of small and low-cost UAVs.

In this dissertation, we assume that the UAVs in an FN are divided into two categories: Flying Access Points (FAPs) and Gateway (GW) UAVs. Although several solutions have been proposed to address the positioning of FAPs, the positioning of GW UAVs has been overlooked in the state of the art. In the following subsections, we review some solutions that have been proposed, as well as some concepts deeply tied with FNs.

2.2.1 Controlled Mobility of the Communications Nodes

As UAVs present high mobility, it can be advantageous to have a central node with holistic information about the state of the network, including the UAVs' positions. This concept was explored by RedeFINE [3], which consists of a routing solution that takes advantage of the centralized view of the FN, available at a Central Station (CS) with holistic knowledge about the network, to define in advance the forwarding tables between UAVs forming a multi-hop network. In RedeFINE, the choice of the paths is based on the smallest cost, defined by the Euclidean distance, and the shortest path is calculated by the Dijkstra's algorithm. For that purpose, the FSPL is used to estimate the Signal-to-Noise Ratio (SNR). The performance evaluation of RedeFINE shows that it achieves better throughput and Packet Delivery Ratio (PDR) than the solutions that it was compared against. The ability to take advantage of the knowledge about the network provided by a central node and the usage of the simplified FSPL model to estimate the SNR in FNs, which were explored by RedeFINE, are important assumptions in the context of this dissertation.

2.2.2 UAV Positioning

In this subsection, we will focus on two types of communications nodes: FAPs and UAV relays. For the positioning of FAPs, several solutions have been proposed [1]. In the following subsection, a reference solution for the FAPs positioning is presented. UAVs working as relay nodes can be used to extend the communications range between two or more ground nodes. The study on the positioning of relay nodes is relevant in the scope of this dissertation to understand how the positions of the UAVs affect the quality of the communications links.

For this problem, solutions like the one presented in [1], where an algorithm named NetPlan is proposed to dynamically determine the FAPs positions according to the users' traffic demands, are worthy of being considered. In NetPlan, the GW UAVs are uniformly distributed around the center of the venue, the FAP-FAP link is modeled by the FSPL model, and the FAP-User link is modeled by the FSPL model with Rician Fast-Fading. The NetPlan algorithm is based on the Potential Fields (PF) technique, where PF Generators are employed to generate force fields that apply forces on the FAPs; these forces can be attractive to areas with high traffic demand, and rejective to areas with lower traffic demand. In order to improve the aggregate throughput, the FAPs closer to the users with higher traffic demands establish smaller Wi-Fi cells, whereas the remaining FAPs establish larger Wi-Fi cells to ensure the overall area coverage. NetPlan provides improvements in the overall QoS metrics, especially for the mean throughput.

A UAV can also be used to enhance the communications range and connectivity between ground nodes. In [8], the effect of the asymmetrical positioning of a UAV between two ground nodes on the network performance is studied. The authors take into consideration the four different coding schemes used in IEEE 802.11b, for which the range increases as lower rates are used, as depicted in Fig. 2.1.

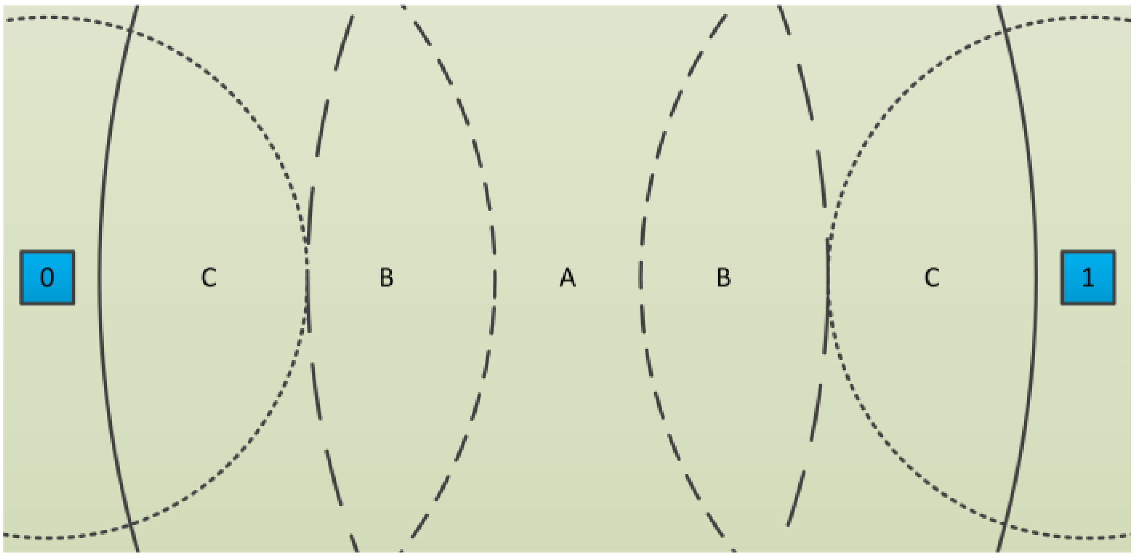

Figure 2.1: Communications link rate range for two IEEE 802.11b nodes [8].

Three possible scenarios can occur when moving the relay node from the equidistant position between the two ground nodes to a non-equidistant position: 1) the link rate to the farther ground node is reduced, while the rate of the other link is not improved; 2) the link rate to the nearer ground node is improved without reducing the rate of the link to the node further away; 3) the rate to the nearest node is improved, while the rate of the link to the further apart node is decreased. To estimate the expected performance for each position, the following algorithm was used: 1) based on the node positions, the distance of the two links L between the ground nodes and the UAV is calculated; 2) for each L, the link rate is estimated; 3) based on empirical link rate combination results, the expected throughput is estimated. The authors were able to achieve favorable outcomes for asymmetrical positioning of the relay node in some situations; one of them increased the end-to-end throughput by 35%, compared to the central position. Hereupon, the altitude of the relay and the horizontal separation between the ground nodes were shown to have great influence in end-to-end throughput. However, traffic patterns, traffic demand, and flow priority were not considered in this work.

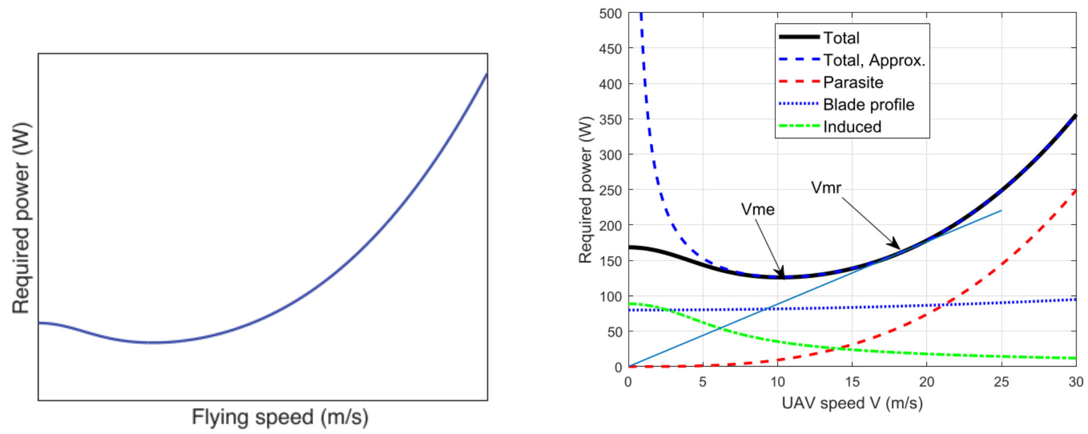

(a) (b)

Figure 2.2: Rotary Wing: Flying Speed vs. UAV Power Consumption [6][9].

2.2.3 Energy in Flying Networks

Unlike ground-based networks, whose communications nodes are typically connected to the electrical grid, FNs composed of UAVs do not have an always-on power supply; therefore, they are dependent on the capacity of the on-board UAV's battery. This, obviously, puts a strain on the total time the FN can be operational. There are two main components in the total energy consumption of a UAV: 1) propulsion energy, which refers to the mechanical energy wasted for movement and hovering – usually, in the order of one kilowatt; and 2) energy used for communications, which is typically used for signal transmission and processing, and computations – usually, in the order of one watt or less.

In [9], the relation between the propulsion power consumption and the UAV flying speed, for both fixed-wing and rotary-wing UAVs, is presented. Fig. 2.2 and Fig. 2.3 [6] represent the power consumption behavior for rotary-wing UAVs, while Fig. 2.4 represents the behavior for fixed-wing UAVs.

2.2.3.1 Rotary-Wing UAV

As it is highly unlikely that both studies have used the exact same model of UAV, by comparing both Fig. 2.2 (a) and Fig. 2.2 (b), we can verify that rotary-wing UAVs have the same type of behavior in terms of power consumption. In Fig. 2.2 (b), for comparison, we should only pay attention to the solid black line (Total), as it is the one that represents the same as Fig. 2.2 (a). Also, still in Fig. 2.2 (b), there are two different speeds that are pointed out for the reader: V_{me} and V_{mr}. The authors define V_{me} as the optimal UAV speed that maximizes the UAV endurance for any given onboard energy, and V_{mr} as the optimal UAV speed that maximizes the total traveling distance for any given onboard energy.

As expected, the higher the velocity of the UAV, the more power it requires. This is true except for very low and null (hovering) speeds, which present a different behavior, as null velocity

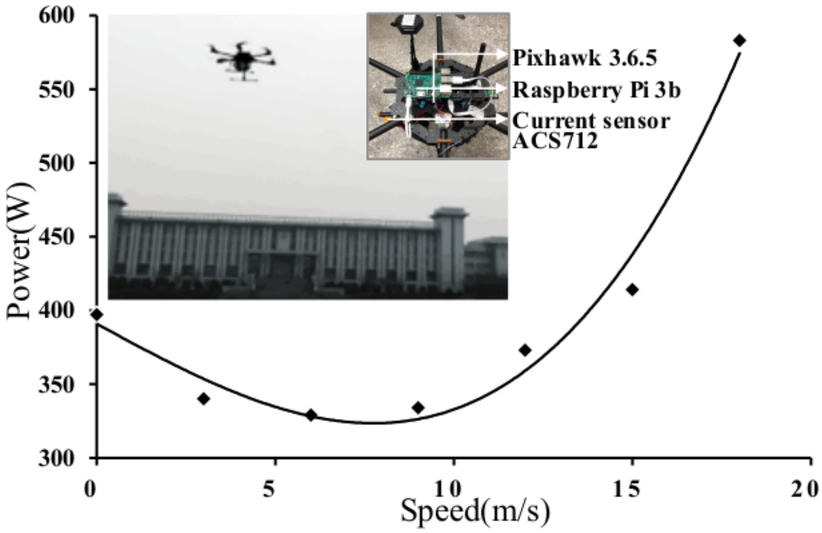

Figure 2.3: Rotary-Wing: Results obtained through real-world tests [10].

requires more power than flying at low speeds. From the behavior showed, we can conclude that moving a Rotary-Wing UAV at too low or too high speeds is not energy-efficient. The high amount of power that rotary-wing UAVs require for traveling at very high speeds makes them not the most suitable for operation in wide geographic areas, as the act of traversing the entire area in a short amount of time would significantly decrease their flying time.

The behavior demonstrated in both plots of Fig. 2.2 was obtained through theoretical modeling. On the other hand, in [10], an experimental speed-aware energy consumption model based on measurements collected in a real-world flight test was built. To perform the flight tests, the authors let the UAV fly along a straight line for no longer than 1000 m, varying the speed from 0 m/s to 18 m/s with a step of 3 m/s. In Fig. 2.3, the results of this real-world flight test are presented; we can observe that, like in the theoretical models, the UAV power consumption is related to the speed through a convex function.

2.2.3.2 Fixed-Wing UAV

Fixed-Winged UAVs do not have the capacity to hover; in Fig. 2.4, this is made evident by defining that for a fixed-wing UAV to be able to hover its energy consumption would be infinite. Overall, the general behavior of energy consumption is similar to that of rotary-wing UAVs: intermediate speed values require less energy than too low or too high flying speeds. However, by comparing the figures for both types of UAVs, it is possible to conclude that fixed-winged UAVs are more capable of traveling long distances, since they spend less energy than rotary-wing UAVs to achieve high values of flying speed, making them more suitable to fly over wide geographic areas.

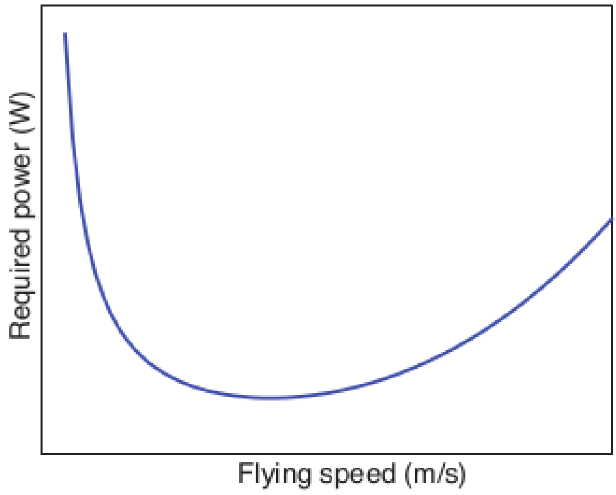

Figure 2.4: Fixed Wing: Flying Speed vs UAV Power Consumption [9].

2.2.3.3 Trajectory movement with Fixed-Wing UAV

As mentioned previously, fixed-wing UAVs do not have the capacity to hover in a position, and the energy consumed in different movements has already been studied in some depth. In [11], a circular motion for the UAV is studied; here, the UAV was acting as a relay between two stationary ground nodes. The energy-efficiency metric is defined as the ratio of the network capacity to the power consumption for both maneuvering and communications. For the evaluation of their solution, the authors defined different radius starting from what would be the ideal position in hovering for maximum network capacity. The authors' solution is named Energy-Efficient Maneuvering and Communication (EEMC), and it was tested against two approaches: capacity maximization and communication (CMMC), and power minimization maneuvering and communication (PMMC). The CMMC approach defines the smaller radius for the circular movement of the relay, thus achieving maximum network capacity. On the other hand, the PMMC approach defines the highest radius for the circular movement, while satisfying the minimum requirement for the network capacity. The EEMC approach radius falls somewhere between the radius defined for EEMC and the radius defined for PMMC. The main conclusions drawn from this study are that for circular trajectories with fixed-winged UAVs, the larger the radius, the lower the power consumption. However, this leads to significant losses in network capacity, due to higher distances from the source.

2.2.3.4 Effect of UAV Altitude in Power Consumption

[12] details an energy-efficient UAV deployment problem while considering flight dynamics and QoS of the users to be served. In terms of flight dynamics, the effects of altitude, UAV components, and payload weight in power consumption during hovering are studied. For altitude, it is stated that the higher the UAV is, the more power it consumes. This happens because as the UAV increases altitude, the air density decreases. When air density decreases, for the UAV to keep the thrust

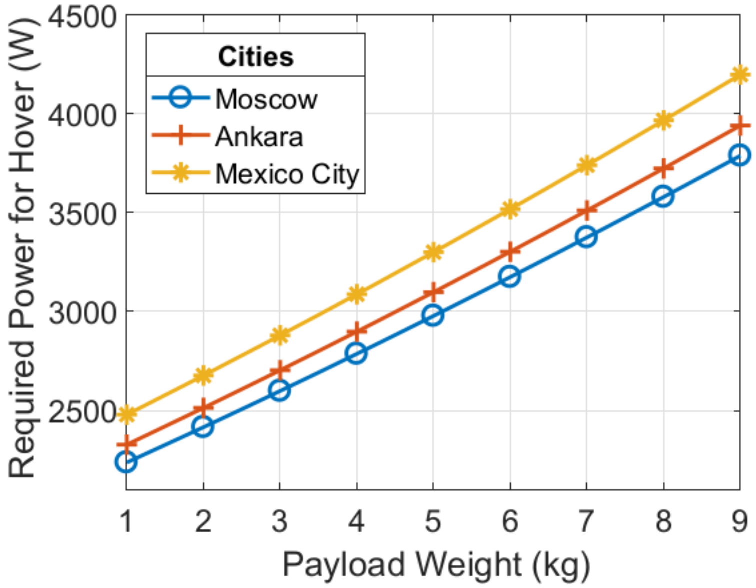

Figure 2.5: Required Power for Hovering vs. Payload Weight [12].

constant, the induced air velocity needs to increase, and for this to happen, the propeller needs to increase the blade tip speed, thus increasing the power consumed. It is concluded that a higher payload weight leads to an increase in power consumption, as more power is required to keep the UAV airborne.

Fig. 2.5 depicts the power required for hovering with different payload weights, in different cities. The authors define the hovering altitudes for different cities: in Moscow, altitude is 124 m, Ankara is 938 m, and Mexico City is 2240 m. As it is possible to conclude from Fig. 2.5, the power required for hovering rises substantially for higher altitudes. Therefore, the altitude of the UAVs should be taken into account when energy efficiency is a concern.

2.2.3.5 Energy Efficiency

[9] presents several trade-offs for UAV-Enabled Wireless Networks, including throughput and energy. They define that this trade-off in traditional wireless communications is rooted in Shannon's capacity formula, which explicitly suggests that the achievable rate increases monotonically with the transmission power. A useful performance metric for this trade-off is energy efficiency, which measures the number of information bits that can be transmitted by using a Joule of energy. However, for UAV-Enabled Wireless Networks we have to take into consideration the propulsion energy; as a result, the energy efficiency should be defined in terms of information bits per Joule of propulsion energy.

In [7], an energy-aware 3D UAV deployment solution is proposed, with the goal of optimizing the network throughput. Here, the trade-off between flight altitude, energy expense, and travel time is addressed. Both radio communications power and maneuvering power are considered as major energy consumers. For maneuvering power, it is demonstrated that moving at high speeds consumes more power than hovering, whereas hovering requires more power than climbing in altitude. Five performance metrics were evaluated: 1) total amount of data transmitted by UAVs; 2) average flight time per UAV; 3) average service time per UAV; 4) service power ratio; and 5) energy efficiency. The proposed solution was compared with two different approaches: 1) User-Aware Approach with a Random Altitude Assignment (UARA), in which the UAV moves to places with high user density and chooses their altitude randomly; and 2) User-Aware Approach with a Minimum Altitude Assignment (UAMA), which is similar to the previous one, with the exception that the UAV flies at the minimum altitude level. The proposed solution achieves better performance in all the metrics that were evaluated.

2.3 Gateway Positioning

In this section, reference solutions for gateway positioning in wireless mesh networks and flying networks are presented.

2.3.1 Wireless Mesh Networks

For FNs, there is not much work done addressing the challenge of gateway positioning. However, for Wireless Mesh Networks (WMNs) in general, there are several studies conducted on the subject. In [13], a survey on gateway selection and gateway positioning algorithms was conducted, separating the algorithms in several categories. They are categorized in terms of 1) channel assignment (Static or Dynamic); 2) Channel-Radio Association (Single-Radio Single-Channel (SRSC), Single-Radio Multi-Channel (SRMC), or Multi-Radio Multi-Channel (MRMC)); 3) Architectures (Centralized, Hybrid or Distributed); and 4) Optimization Techniques (Operation Research, Meta-heuristic or Heuristic). In Figures 2.6, 2.7, 2.8, and 2.9, the division of the algorithms inside each of the four categories is presented.

From the previously mentioned figures, it is possible to conclude what are the parameters that most of the solutions for WMNs take into consideration. However, good outcomes of these solutions tailored for WMNs may not be directly translated into good outcomes in FNs, as there are several aspects that are not considered, like nodes mobility. When categorizing the solutions by architecture, we can see that both hybrid and centralized solutions are in high number; in fact, a centralized solution for FNs can be useful, as having a node with the full knowledge about the network can help, for instance, in preventing interference between the UAVs. Now, observing the evaluation by network parameters in Fig. 2.9, it is obvious that power is not one of the main topics of interest; this may happen because WMNs are typically connected to the electrical grid; thus the lifetime of the network is not a concern.

In [14], another survey regarding gateway positioning in WMNs is presented. It is possible to conclude that algorithms that deal with load balancing and cost minimization are irrelevant to this

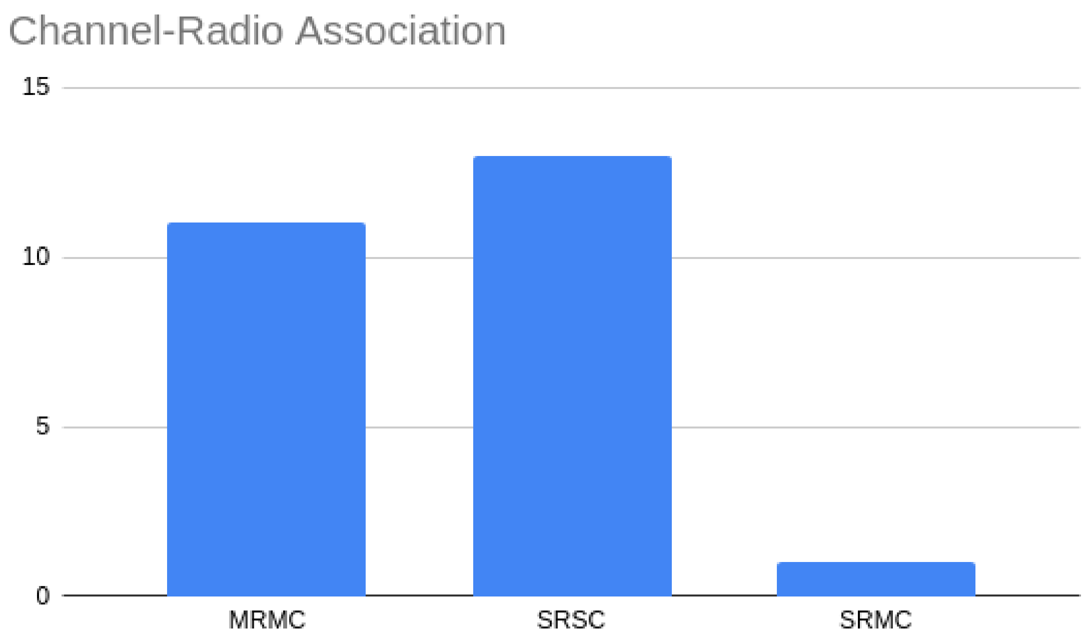

Figure 2.6: Evaluation by Channel-Radio Association.

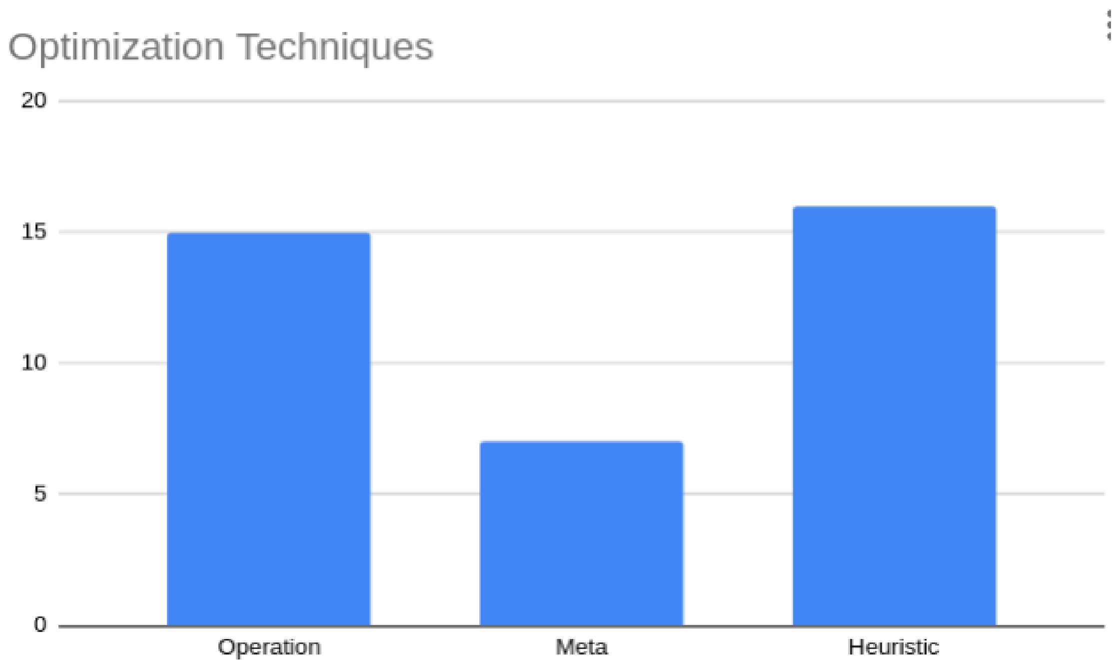

Figure 2.7: Evaluation by Optimization Techniques.

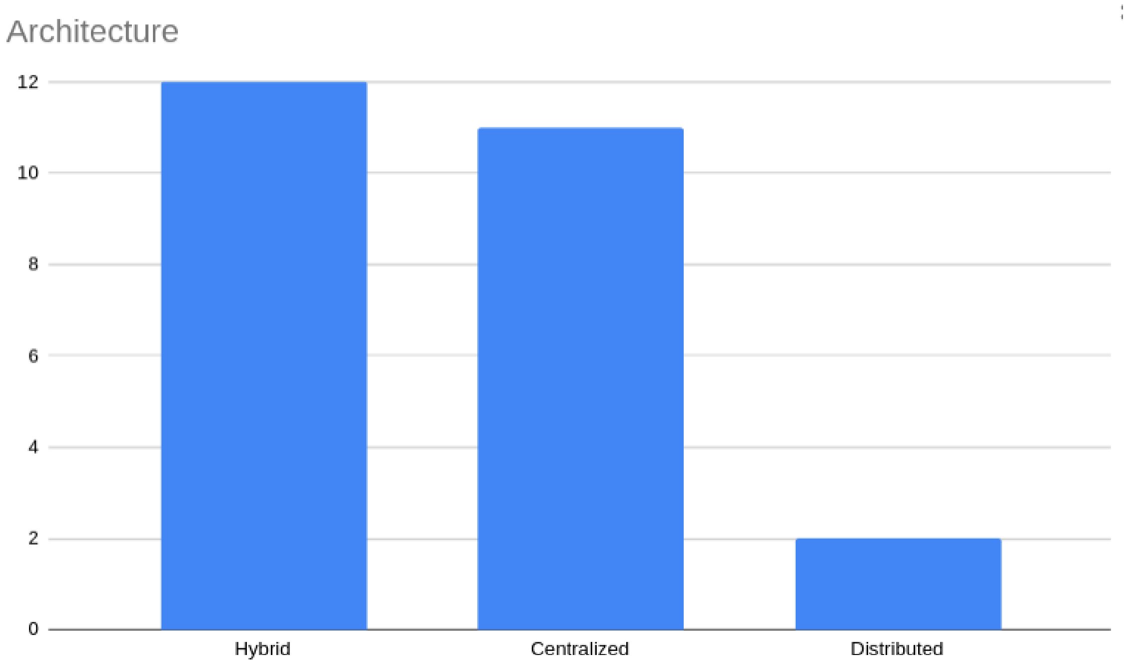

Figure 2.8: Evaluation by Architecture.

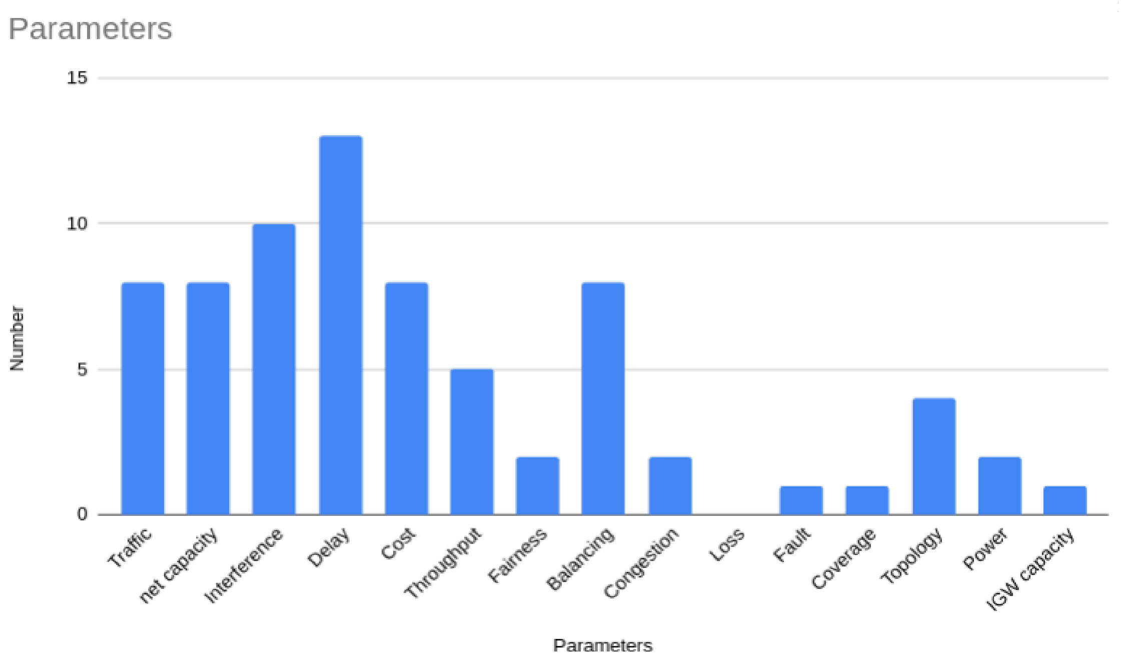

Figure 2.9: Evaluation of network performance metrics.

dissertation, since their main objective is to reduce the number of gateways. This dissertation is focused on a single GW UAV.

In [15], positioning approach for a single gateway in WMNs is proposed. The authors aim at maximizing the minimum flow throughput that can be achieved by appropriately configuring the network in terms of the set of links to activate, their physical layers parameters, and the flow routes. Their strategy was tested with four different types of networks: Grid, Regular Sub-Compact Grids, Arbitrary Networks, and Irregular Grid Networks. They proposed three different heuristics, from now on named H1, H2, and H3. H1 is based on the minimum hop metric. H2 selects the position by guaranteeing that every node has the minimum power required. H3 uses Signal-to-Interference-plus-Noise Ratio (SINR) as the metric, and applies the shortest path algorithm to compute the minimum weight path from any node to the location of the gateway; the position is selected by the lowest sum of the weights, considering all the shortest paths from all the nodes to that position. This strategy has presented better performances for both H1 and H3, but for H2 it presents sub-optimal performance due to selecting the same position regardless of the transmission powers. Despite both H1 and H3 present good performance, H3 is better because it selects only a single gateway position, while H1 presents a list of possible gateway positions.

In [16], an algorithm for gateway positioning optimization based on Load Balancing is presented. The authors have three main objectives: reduce the number of gateways, reduce the average Mesh Router (MR)-GW hop count, and balance the load among gateways. They proposed a two-stage algorithm: the first stage consists of gateway selection, and the second stage consists of MR attachment. Gateway selection algorithm looks for the minimal number of nodes such that their neighborhoods cover all the nodes. This solution was compared with Degree based Greedy Dominating Tree Set Partitioning (GDTSP) and Weight-based GDSTP, and it achieves better load balance; however, for both the number of gateways and average MR-GW hop count, it achieves the same performance.

In [17], a two-phased algorithm named Split-Merge-Shift (SMS) is presented. The first phase consists of selecting the initial candidate based on the highest network density, where the nodes at one hop of distance are added to the cluster until every node has a role. Then, it goes to the merge operation, where neighboring clusters are merged, forming clusters with stronger bonds. The next stage consists of the split operation, where the smallest cluster is broken to have a better chance of merging with other clusters; but, if this operation creates a larger number of clusters, the previous state is restored. The next stage is the shift operation, which is used for single clusters that can not merge. If, after the split, merge, and shift steps, the solution set is larger, then the algorithm stops and returns to the previous state; this is the stop condition of the SMS algorithm. SMS was evaluated in terms of the number of gateways it produces, cluster size variation, and maximum and average relay loads. It was able to achieve a reduction in the number of gateways produced by 30% while producing uniform clusters.

2.3.2 Flying Networks

As mentioned before, there is not much work done addressing the positioning of the GW UAV in FNs. Only recently has this issue started being addressed. In [4], a traffic-aware GW UAV Placement (GWP) algorithm for FNs with controlled topology is proposed. Here, a CS is responsible for 1) defining the positions of the FAPs by running the NetPlan algorithm [1]; 2) calculating the forwarding tables to be used by the FAPs by running RedeFINE [3]; and 3) positioning the GW UAV to enable links able to accommodate the FAPs' traffic demand by running GWP [4]. Taking into consideration the future positions of the FAPs and the bitrate of the generated traffic flows, the GWP algorithm aims at guaranteeing that the wireless link between each FAP and the GW UAV has a minimum SNR that enables the usage of the minimum Modulation and Coding Scheme (MCS) index able to accommodate the traffic demand. The FSPL model is used to estimate the SNR of the wireless links and to determine the maximum distance between each FAP and the GW UAV. The maximum distance in the three-dimensional space corresponds to the radius of a sphere, centered at each FAP, inside which the GW UAV should be placed. Considering all the FAPs in the network, the position of the GW UAV corresponds to the subspace generated by the intersection of the spheres. To calculate this subspace, the GWP algorithm is followed, which iteratively allows calculating the optimal point for positioning the GW UAV and the transmission power.

The GWP algorithm was evaluated by means of ns-3 simulations under two distinct networking scenarios: a simple one with 4 FAPs all equidistant from each other (Figure 2.11), and a complex scenario, in which 10 FAPS were randomly positioned in order to form two zones with different traffic demand (Figure 2.12). In both of them, the baseline corresponds to the GW UAV placed in the FAPs center.

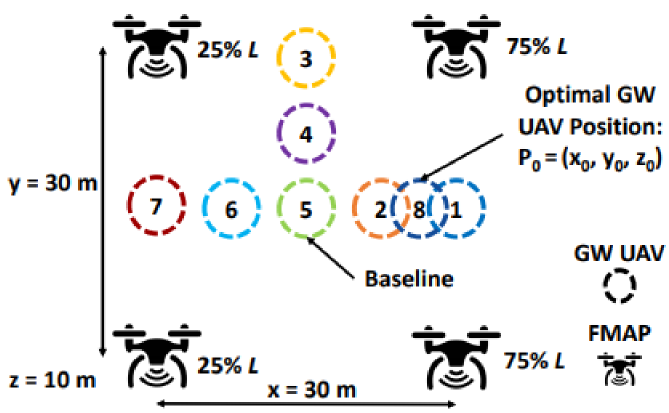

Figure 2.10: Simple scenario used to evaluate the GWP algorithm [4].

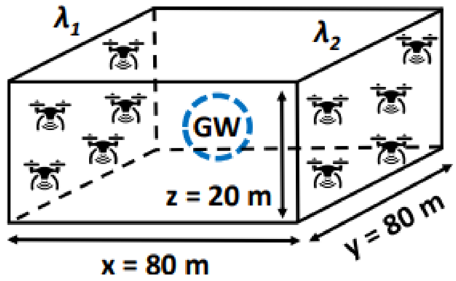

Figure 2.11: Complex scenario used to evaluate the GWP algorithm [4].

The performance of GWP was evaluated considering two performance metrics: aggregate throughput, which is the mean number of bits received per second by the GW UAV, and end-to-end delay, which it is the time taken by the packets to reach the application layer of the GW UAV since the instant they were generated by the FAPs. For both scenarios, the GWP algorithm was able to achieve better results for both metrics when compared to the baseline. The obtained results show that it is possible to improve the performance of the FNs by dynamically adjusting the position of the GW UAV, considering both the positions and the offered traffic of the FAPs. However, the energy consumption of the GW UAV is not considered, as the GW UAV hovers in the optimal position; it was previously shown in this chapter that hovering is not the most energy-efficent behavior.

2.4 Summary and Main Conclusions

From the content that was exposed in the previous sections, it is possible to draw important conclusions in the context of this dissertation:

- The usage of UAVs carrying communications nodes able to provide Internet access is a subject of increasing research interest.
- Equidistant positioning of a communications node may not always be the ideal solution, as asymmetrical positioning has achieved favorable outcomes for heterogeneous traffic demand. [8].
- The energy consumption for movement in rotary-wing UAVs does not have an uniform behavior: it decreases for low-velocity values, and then it starts increasing as velocity increases. From this, it is possible to conclude that hovering is not the most energy-efficient state.
- The traffic demand of the FAPs should be considered when tackling the issue of GW UAV positioning, as a traffic-aware solution has achieved improved results.
- There is a clear lack of GW UAV positioning solutions that deal with the issue of minimizing the energy consumption of the GW UAV.

Chapter 3

Energy-aware Gateway Positioning Algorithm

The previous chapter was focused on exposing the necessary knowledge and the state of the art solutions that have been considered to solve the problem addressed by this dissertation. In this chapter, we present the proposed Energy-aware GateWay Positioning (EGWP) algorithm, including the system model and problem formulation.

3.1 System Model and Problem Formulation

When deploying a single GW UAV in an FN, which is the communications node responsible for forwarding traffic to/from the Internet, it is important to place the GW UAV taking into account the traffic demand of each FAP providing connectivity to the users on the ground. We assume that the information about the traffic demand is provided by a CS, which is a centralized node in charge of defining the positions of the FAPs by running a state of the art FAPs positioning algorithm [1], thus providing a holistic knowledge of the network. Here, we assume that two types of UAVs compose the FN: 1) FAPs, which were described previously as the nodes that provide Internet access to ground nodes; and 2) a single GW UAV, which is the communications node responsible for forwarding the traffic to/from the Internet. These elements and the way they interact are depicted in Fig. 3.1. The number of FAPs may increase; however, a single GW UAV is always considered.

When planning an FN, unlike grid-connected networks, the limited onboard energy of the UAV worths being taken into consideration, as it restricts the total amount of time the network can remain operational. A longer lasting FN will be able to satisfy its users for a longer time, thus increasing the network availability. Typically, in the state of the art UAV positioning solutions, once both FAPs and GW UAVs reach the optimal position, they simply hover in that position. However, it was proven that hovering is not the most energy efficient behavior that a UAV can adopt, since UAVs moving at relatively low speeds consume less energy than hovering [9][6].

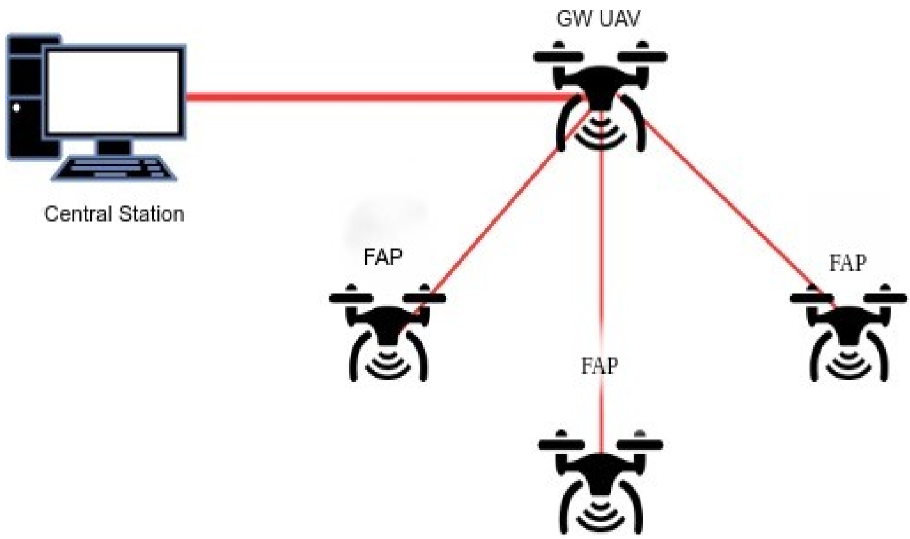

Figure 3.1: System Elements.

For these reasons, an algorithm that allies the positioning of the GW UAV taking into consideration the different traffic demands of all FAPs, while maintaining an energy efficient behavior, is worth to be considered to improve the overall performance of the FN.

We assume that the wireless links between the FAPs and the GW UAV are modeled by the FSPL [18] model presented in (3.1), since there is a strong Line of Sight (LoS) component between UAVs flying dozens of meters above the ground.

$$\frac{P_r}{P_t} = \left[\frac{\lambda}{4\pi r}\right]^2 \tag{3.1}$$

In (3.1), P_r stands for the power received at the GW UAV, P_t is the transmission power of each FAP, the wavelength λ is equal to c/f, where c is the speed of light in vacuum and f is the carrier frequency, and r represents the distance between the transmitter and receiver UAVs. We assume that the maximum channel capacity is equal to the data rate associated with the Modulation and Coding Scheme (MCS) index selected by the nodes; this information is provided in Fig. 3.2. Each MCS index requires a minimum value of $SNR = P_r/N_0$, which is derived from P_r considering a constant noise power N_0. The wireless medium is shared, so we assume that every UAV can listen to the other UAVs. For Medium Access Control (MAC), the Carrier Sense Multiple Access with Collision Avoidance (CSMA/CA) is employed.

802.11ac - VHT MCS, SNR and RSSI

VHT MCS	Modulation	Coding	20MHz				40MHz				80MHz				160MHz			
			Data Rate		Min. SNR	RSSI	Data Rate		Min. SNR	RSSI	Data Rate		Min. SNR	RSSI	Data Rate		Min. SNR	RSSI
			800ns	400ns			800ns	400ns			800ns	400ns			800ns	400ns		
1 Spatial Stream																		
0	BPSK	1/2	6.5	7.2	2	-82	13.5	15	5	-79	29.3	32.5	8	-76	58.5	65	11	-73
1	QPSK	1/2	13	14.4	5	-79	27	30	8	-76	58.5	65	11	-73	117	130	14	-70
2	QPSK	3/4	19.5	21.7	9	-77	40.5	45	12	-74	87.8	97.5	15	-71	175.5	195	18	-68
3	16-QAM	1/2	26	28.9	11	-74	54	60	14	-71	117	130	17	-68	234	260	20	-65
4	16-QAM	3/4	39	43.3	15	-70	81	90	18	-67	175.5	195	21	-64	351	390	24	-61
5	64-QAM	2/3	52	57.8	18	-66	108	120	21	-63	234	260	24	-60	468	520	27	-57
6	64-QAM	3/4	58.5	65	20	-65	121.5	135	23	-62	263.3	292.5	26	-59	526.5	585	29	-56
7	64-QAM	5/6	65	72.2	25	-64	135	150	28	-61	292.5	325	31	-58	585	650	34	-55
8	256-QAM	3/4	78	86.7	29	-59	162	180	32	-56	351	390	35	-53	702	780	38	-50
9	256-QAM	5/6			31	-57	180	200	34	-54	390	433.3	37	-51	780	866.7	40	-48
2 Spatial Streams																		
0	BPSK	1/2	13	14.4	2	-82	27	30	5	-79	58.5	65	8	-76	117	130	11	-73
1	QPSK	1/2	26	28.9	5	-79	54	60	8	-76	117	130	11	-73	234	260	14	-70
2	QPSK	3/4	39	43.3	9	-77	81	90	12	-74	175.5	195	15	-71	351	390	18	-68
3	16-QAM	1/2	52	57.8	11	-74	108	120	14	-71	234	260	17	-68	468	520	20	-65
4	16-QAM	3/4	78	86.7	15	-70	162	180	18	-67	351	390	21	-64	702	780	24	-61
5	64-QAM	2/3	104	115.6	18	-66	216	240	21	-63	468	520	24	-60	936	1040	27	-57
6	64-QAM	3/4	117	130.3	20	-65	243	270	23	-62	526.5	585	26	-59	1053	1170	29	-56
7	64-QAM	5/6	130	144.4	25	-64	270	300	28	-61	585	650	31	-58	1170	1300	34	-55
8	256-QAM	3/4	156	173.3	29	-59	324	360	32	-56	702	780	35	-53	1404	1560	38	-50
9	256-QAM	5/6			31	-57	360	400	34	-54	780	866.7	37	-51	1560	1733.3	40	-48
3 Spatial Streams																		
0	BPSK	1/2	19.5	21.7	2	-82	40.5	45	5	-79	87.8	97.5	8	-76	175.5	195	11	-73
1	QPSK	1/2	39	43.3	5	-79	81	90	8	-76	175.5	195	11	-73	351	390	14	-70
2	QPSK	3/4	58.5	65	9	-77	121.5	135	12	-74	263.3	292.5	15	-71	526.5	585	18	-68
3	16-QAM	1/2	78	86.7	11	-74	162	180	14	-71	351	390	17	-68	702	780	20	-65
4	16-QAM	3/4	117	130	15	-70	243	270	18	-67	526.5	585	21	-64	1053	1170	24	-61
5	64-QAM	2/3	156	173.3	18	-66	324	360	21	-63	702	780	24	-60	1404	1560	27	-57
6	64-QAM	3/4	175.5	195	20	-65	364.5	405	23	-62			26	-59	1579.5	1755	29	-56
7	64-QAM	5/6	195	216.7	25	-64	405	450	28	-61	877.5	975	31	-58	1755	1950	34	-55
8	256-QAM	3/4	234	260	29	-59	486	540	32	-56	1053	1170	35	-53	2106	2340	38	-50
9	256-QAM	5/6	260	288.9	31	-57	540	600	34	-54	1170	1300	37	-51			40	-48

Figure 3.2: MCS index information for the IEEE 802.11ac technology [19].

The power consumed by the UAV for its propulsion is defined in [6] as having three components:

- **Blade Profile**, which is the power required to overcome the profile drag of the blades;
- **Induced**, which is required to overcome the induced drag of the blades;
- **Parasite**, required to overcome the fuselage drag.

The equation for calculating the power P consumed by the UAV while moving at speed V is given in (3.2).

$$P(V) = P_b \left(1 + \frac{3V^2}{U_{tip}^2}\right) + P_{ind} \left(\sqrt{1 + \frac{V^4}{4v_0^4}} - \frac{V^2}{2v_0^2}\right)^{3/2} + \frac{1}{2} d_0 \rho s A V^3 \tag{3.2}$$

In (3.2), the first addend represents the blade profile power in the hovering state, and U_{tip} denotes the tip speed of the rotor blade. The second addend represents the induced power component, where P_{ind} is a constant representing the induced power in the hovering state, and v_o is the mean rotor induced velocity in the hovering state. The third addend represents the parasite component, where d_0 is the fuselage drag ratio, s represents the rotor solidity, ρ denotes the air density, and A represents the rotor disc area. These parameters can be obtained from the UAV specifications, with the exception of ρ, whose value depends on the environment. The analysis of (3.2) made in [6] shows that there is a range of UAV speeds V for which the power consumed by the UAV is lower than the power consumed for hovering. This behavior is depicted in Fig. 3.3.

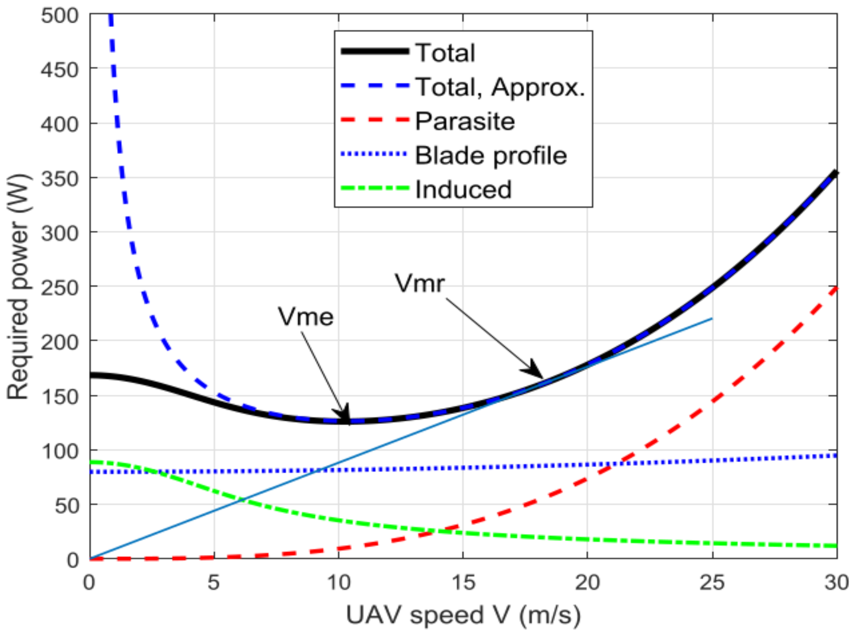

Figure 3.3: Propulsion power consumption versus UAV speed V [6].

The reference scenario considered from now on is presented in Fig. 3.4.

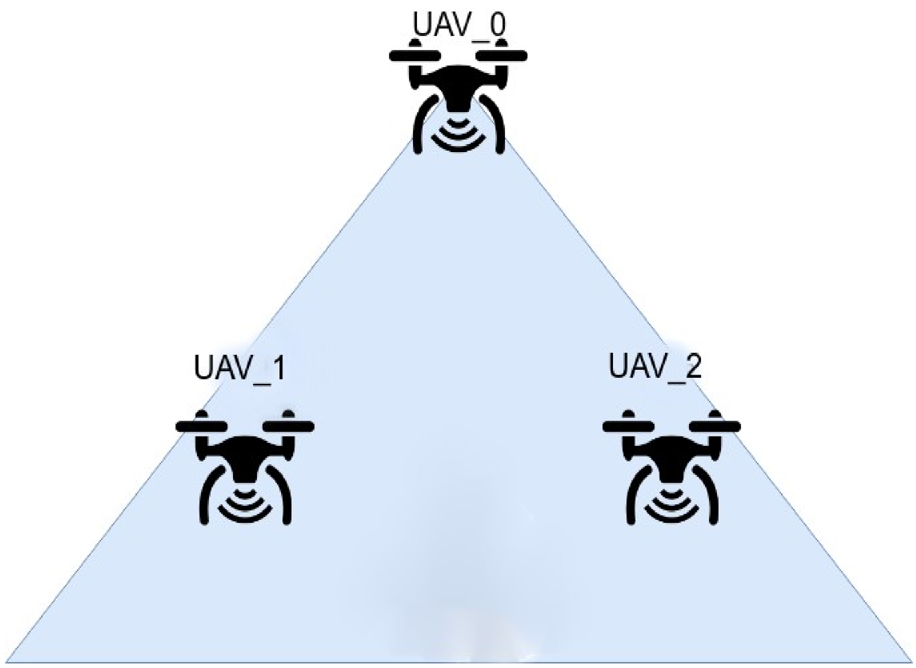

Figure 3.4: Reference scenario.

In our problem, the FN is modeled as a directed graph $G = (U, L)$, where $U = \{UAV_0, ..., UAV_{N-1}\}$ is the set of UAVs i positioned at $Q_i = (x_i, y_i, z_i)$ and $L \subseteq U \times U$ is the set of directional links between UAVs i and j, with $(i, j) \in L$ and $i, j \in U$.

Let us assume that each UAV_i $i \in \{1,...,N-1\}$, performs the role of FAP and transmits a traffic flow $F_{0,i}$ towards UAV_0, which performs the role of GW UAV. In this sense, we have a tree $T(U, L_T)$ that is a subgraph of G, where $L_T \subset L$ is the set of direct links between each UAV_i and UAV_0. This tree defines the FN active topology, which is composed of single-hop paths.

We aim at determining the trajectory $Q_0(t) = [x_0(t), y_0(t), z_0(t)]$ of UAV_0, to be completed at a velocity up to V_{max}, such that the power $P_0(t)$ consumed by the UAV_0 is minimal and the transfer of all traffic flows $F_{0,i}$ with bitrate T_i, in bit/s, is guaranteed. We also have to guarantee that the throughput $R_i(t)$ is not higher than the offered T_i. Our objective function is defined in 3.3a.

$$\text{minimize} \quad \int_0^t P_0(t)dt \tag{3.3a}$$

$$\text{subject to:} \quad \frac{dQ_0(t)}{dt} \leq V_{max} \tag{3.3b}$$

$$Q_0(t) \neq (x_i, y_i, z_i), i \in \{1,...,N-1\} \tag{3.3c}$$

$$R_i(t) \leq T_i, i \in \{1,...,N-1\} \tag{3.3d}$$

$$T_i > 0, i \in \{1,...,N-1\} \tag{3.3e}$$

$$z_i \geq 0, i \in \{0,...,N-1\} \tag{3.3f}$$

$$(0,i),(i,0) \in L_T, i \in \{1,...,N-1\} \tag{3.3g}$$

3.2 Energy-aware Gateway Positioning algorithm

As previously mentioned, there is a range of UAV speeds wherein the UAV consumes less power than when it is hovering. This assumption is the basis of the Energy GateWay Positioning (EGWP) algorithm proposed in this dissertation. The EGWP algorithm was built upon the GWP algorithm proposed in [4]. GWP takes advantage of the knowledge of the FAPs positions and their traffic demands, which is provided by a state of the art FAP positioning algorithm such as the one presented in [1]. Then, the position of the GW UAV that maximizes the aggregated throughput between the FAPs and the GW UAV is defined. The EGWP algorithm improves the GWP algorithm by considering the power consumption of the GW UAV. Instead of just hovering in the optimal position defined by the GWP algorithm, with EGWP the GW UAV moves along a trajectory at the speed that minimizes the power consumed, without compromising the network performance.

The first step of the EGWP algorithm consists of determining the minimum SNR_i that enables the usage of an MCS index MCS_i capable of accommodating the traffic demand T_i, in bit/s, offered by FAP_i (line 1 of Alg. 1). For that purpose, the relation between the SNR and the fair share of the wireless channel capacity is considered, following the rationale proposed in [4]. The fair share is defined as the maximum capacity of the wireless link between each FAP and the GW UAV, which is assumed to be equal to the data rate of the MCS_i index over the number of FAPs sharing the medium. The minimum SNR_i required for using MCS_i imposes a minimum received power P_{r_i}. Then, considering a transmission power P_{t_i} set to 20 dBm, EGWP calculates the maximum transmission range r_i for FAP_i for achieving the minimum SNR_i, as presented in Fig. 3.5 (line 2 of Alg. 1); we assume that P_{t_i} is equal for all FAPs. In the three-Dimensional (3D) space, r_i represents the radius of a sphere centered at FAP_i. Then, EGWP finds the volume that results from the intersection of the spheres centered at each FAP_i; an example of this volume is illustrated in Fig. 3.5. The intersection between the spheres defines the volume within which the GW UAV can move without compromising the QoS. If no intersection is found, the algorithm is terminated (line 5 of Alg. 1), as it constitutes an issue of network planning and not gateway positioning. Otherwise, the altitude corresponding to the highest area inside the intersection volume is selected (line 9 of Alg. 1). A constant altitude is defined since changes in the UAV altitude imply higher power consumption [12]. The centroid of that area is the optimal position, where all possible trajectories for the GW UAV will pass through (line 10 of Alg. 1).

The next step consists in defining the waypoints for the possible trajectories. EGWP computes three possible trajectories and five waypoints for each trajectory. An example of the three trajectories computed is given in Fig. 3.6. For the first trajectory (Fig. 3.6a), apart from the centroid, the waypoints are located in the intersection area with the highest and lowest values of x in both extremes of the y-axis (line 11 of Alg. 1). For the second trajectory (Fig. 3.6b), the waypoints are located in the intersection area with the highest and lowest values of y in both extremes of the x-axis (line 12 of Alg. 1). For the third trajectory (Fig. 3.6c), the waypoints are defined as the four extreme points in the area of intersection that have the same x or y coordinate as the centroid (line 13 of Alg. 1). The selected trajectory is the one that has the highest total sum of distances between successive waypoints (line 14 of Alg. 1), in order to maximize the time the GW UAV is moving at the speed consuming the lowest power. However, as an area of intersection of great dimensions may lead to the decrease in network performance, due to SNR degradation, an SNR margin was defined so that when the trajectory to be performed is long, which is directly proportional to the size of the area of intersection, the SNR between each FAP and the GW UAV will be increased, ; this will result in a smaller intersection area. With this in mind, if the trajectory distance is higher than or equal to 160 m, then the SNR is increased by 4 dB (line 15 and 16 of Alg.1); if the distance is higher than or equal to 120 m but shorter than 160 m, then the SNR is increased by 3 dB (line 18 and 19 of Alg.1); if the distance is higher than or equal to 80 m but shorter than 120 m, then the SNR is increased by 2 dB (line 21 and 22 of Alg.1). The values used for the SNR margin are adjustable in the algorithm and were obtained on a trial and error basis; their fine-tuning is left for future work. After the SNR is readjusted, the previous steps of the algorithm are executed again. The trajectory is defined by 5 waypoints: the centroid (Pc) and the edges of the area (P1, P2, P3, and P4). The UAV starts in Pc and goes to P1. Afterward, it moves to P2 and then to P3, passing through Pc. Before returning to Pc, the UAV passes through P4.

The UAV hovers for 1 s at each of the waypoints to invert the movement direction. The 1 s hovering is used as an approximation to the energy consumed during the change of direction. This was considered in EGWP because, to the best of our knowledge, there is no model in the state of the art available to characterize the energy consumption for this action of the UAV.

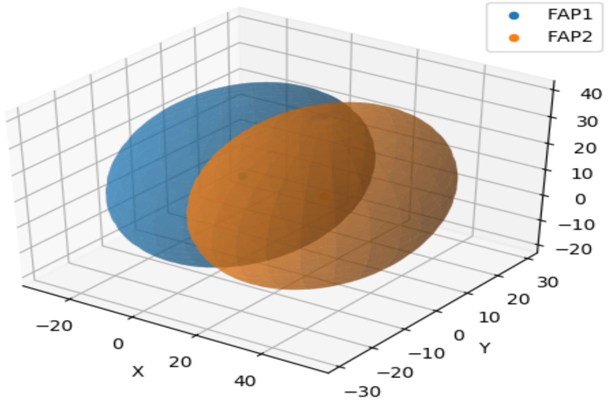

Figure 3.5: Spheres representing the communications range of each FAP, considering the FSPL model, constrained by the SNR value that enables the selection of an MCS index compliant with the traffic demand. The intersection area, within which the GW UAV can move, results from the intersection of the spheres.

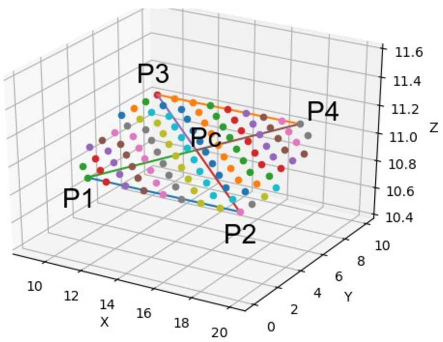

(a) Trajectory 1.

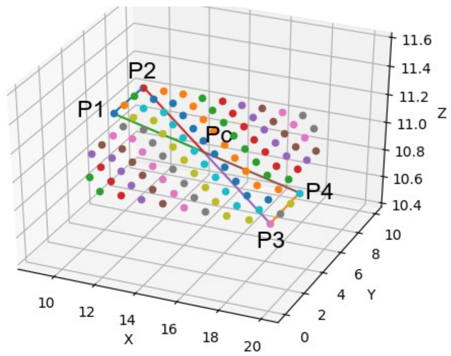

(b) Trajectory 2.

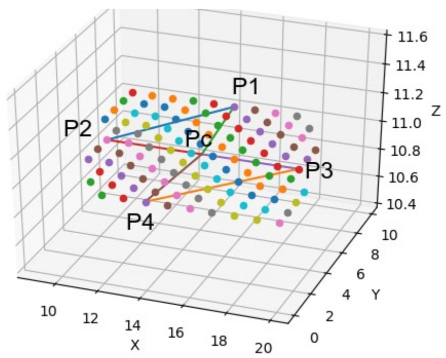

(c) Trajectory 3.

Figure 3.6: Trajectory examples.

Algorithm 1 Energy-aware GateWay Positioning Algorithm

```
1: Set target SNR values for each FAP
2: Calculate the transmission range of each FAP          ▷ Using FSPL model
3: Calculate intersection of transmission ranges
4: if No intersection is found then
5:     Exit
6: else
7:     IntersectionPoints ← Intersection
8: end if
9: DesiredAltitude ← Altitude with more points
10: Find the centroid
11: Define waypoints for the first trajectory
12: Define waypoints for the second trajectory
13: Define waypoints for the third trajectory
14: Selected Trajectory ← maximumDistance(first, second, third)
15: if distanceTrajectory >= 160 then
16:     SNR=SNR+4
17: end if
18: if 160>distanceTrajectory>=120 then
19:     SNR=SNR+3
20: end if
21: if 120>distanceTrajectory>=80 then
22:     SNR=SNR+2
23: end if
24: Repeat from line 2 to line 14
```

3.3 Summary

In this chapter, the problem addressed in this dissertation was presented; it consists of the positioning of a single GW UAV to minimize its energy consumption without compromising the overall network performance. The system elements were presented and described, including the Central Station, the GW UAV, and the FAPs. After these initial remarks, the problem was formulated, and the models and reference scenario considered to illustrate the problem were presented. Lastly, the Energy-aware GateWay Positioning (EGWP) algorithm proposed in this dissertation was presented, and each step of the EGWP was explained in detail.

Chapter 4

UAV Power Simulator

To perform the evaluation of the EGWP algorithm presented in Chapter 3, a custom-tailored simulator was developed in Python [20], named UAVPowerSim. In this simulator, the EGWP algorithm and the power consumption theoretical model presented in (3.2) were implemented. The developed simulator is available in [21]. The simulator was built to evaluate the power consumption when the UAV moves along the trajectory defined by EGWP against the baseline – the GW UAV hovering in the optimal position.

4.1 UAV Power Simulator Input Parameters

The first set of inputs that UAVPowerSim receives are the physical attributes of the UAV and the environment constants, which are the same as those used in [6], and presented in Table 4.1. The second set of inputs are the ones related to the FSPL model, which are the necessary parameters to accurately calculate the area of intersection between the FAPs. With this in mind, in this dissertation, we considered the IEEE 802.11ac technology, 160 MHz channel bandwidth, 5250 MHz (channel 50) as the carrier frequency, and the maximum capacity of the shared wireless medium equal to the data rate of the maximum MCS index of the technology being used: 780 Mbit/s for the IEEE 802.11ac technology, considering a single spatial stream. Another parameter required is the transmission power of the FAPs, which was set to 20 dBm. The last of these parameters is the speed-of-light in the vacuum, $c = 3 \times 10^8$ m/s.

After the inputs of UAVPowerSim are set, it is necessary to read the positions of the FAPs and their traffic demands. This information is read from a text file with a specific structure, which is shown in the following:

```
Number of FAPs:
2
Positions(x,y,z):
0,0,10
0,20,10
Traffic(Mbit/s):
```

Notation	Physical definition	Value
W	UAV weight	20 N
R	Rotor radius	0.4 m
Ω	Blade angular velocity	300 rad/s
k	Incremental correction factor to induced power	0.1
δ	Profile drag coefficient	0.012
ρ	Air density	1.225 kg/m
A	Rotor disc area ($A = \pi R^2$)	0.503 m
U_{tip}	Tip speed of the rotor blade ($U_{tip} \triangleq \Omega R$)	120 m/s
d_0	Fuselage drag ratio	0.6
v_0	Mean rotor induced velocity in hovering state ($v_0 = \sqrt{\frac{W}{2\rho A}}$)	4.03
s	Rotor solidity	0.05
P_b	Blade profile power in hovering state ($P_b \triangleq \frac{\delta}{8}\rho s A \Omega^3 R^3$)	79.86
P_{ind}	Induced power in hovering state ($P_{ind} \triangleq (1+k)\frac{W^{3/2}}{\sqrt{2\rho A}}$)	88.63

Table 4.1: UAV and environment attributes [6].

```
250,250
```

The last setup that needs to be done is the relation between the SNR required for the selection of each MCS index; this was implemented by means of a dictionary that maps the data rate to the minimum SNR required. The maximum data rate achieved is influenced by the number of FAPs in the network, as the fair share for each FAP is assumed to be equal to the data rate of each MCS index over the number of FAPs. The implementation of this last part is shown in the following:

```
    dicMCS=[
    {"SNR":11,"data_rate":58.5/len(x)},
    {"SNR":14,"data_rate":117/len(x)},
    {"SNR":18,"data_rate":175.5/len(x)},
    {"SNR":20,"data_rate":234/len(x)},
    {"SNR":24,"data_rate":351/len(x)},
    {"SNR":27,"data_rate":468/len(x)},
    {"SNR":29,"data_rate":526.5/len(x)},
    {"SNR":34,"data_rate":585/len(x)},
    {"SNR":38,"data_rate":702/len(x)},
    {"SNR":40,"data_rate":780/len(x)}
]
```

4.2 UAV Power Simulator Implementation

After all the initial setup is done, the next step is to calculate the area of intersection between the FAPs. First, it is necessary to calculate the communications range of each FAP, considering the target SNR value that enables the selection of an MCS index compliant with the traffic demand, as presented in Fig. 4.1. The communications range of each FAP is represented as a sphere centered in the FAP itself; the intersection of all spheres corresponds to the desired area of intersection, which is determined as presented in the following:

```
def calculateValidPoints(pd,xmax,ymax,zmax,xd,yd,zd,SNR_values):
    validPoints = []
    dist = [None]*len(x)
    while xd <= xmax:
        yd=min(yToCalcNeg)
        count=0
        while yd <= ymax:
            zd=min(zToCalcNeg)
            count=0
            while zd <= zmax:
                #point to evaluate SNR level
                currentPoint=np.array((xd,yd,zd))
                i=0
                count=0
                while i<len(x):
                    #calculate distance between FAP and point
                    dist[i] = np.linalg.norm(pd[i]-currentPoint)
                    if(dist[i]>0.0):
                        #apply FSPL
                        Pr=Pt+20*math.log10(c/(4*freq*dist[i]*math.pi))
                        #if point is in desirable SNR level
                        if((Pr-noise)>=SNR_values[i]):
                            count+=1
                    dist[i]=None
                    i+=1
                if(count==len(x)):
                    validPoints.append(currentPoint)
                zd+=step
            yd+=step
        xd+=step
    return validPoints
```

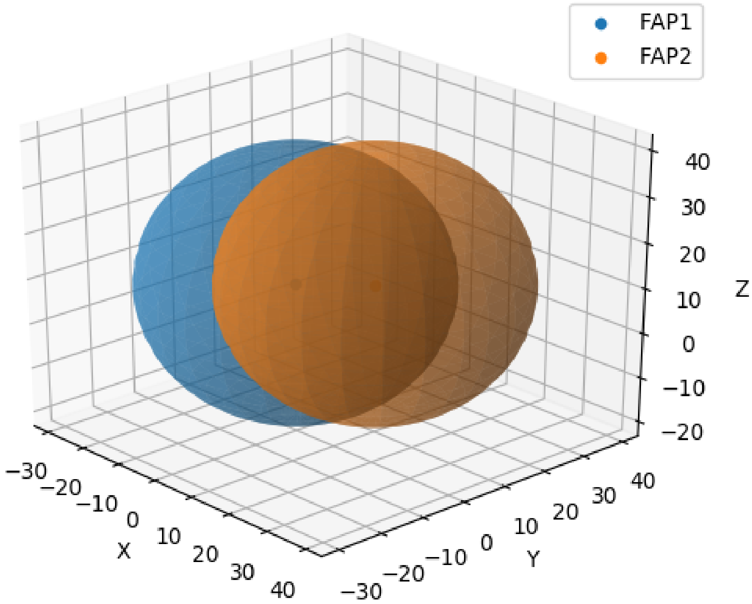

Figure 4.1: Communications range for each FAP and the resulting volume of the intersection.

The function to calculate the area of intersection takes as arguments the coordinates of each FAP (pd list), the maximum values of the coordinates that the communications range of each FAP can achieve (xmax, ymax, zmax), the minimum values (xd, yd, zd), and the SNR required for each FAP (SNR_values list). This function needs the NumPy [22] package to calculate the Euclidean distances.

In order to facilitate the visualization of the intersection between the FAPs, we used the Matplotlib package to generate figures. In Fig. 4.2a, an example of a volume of intersection between two FAPs is depicted. To get the actual intersected area, we need to search in the volume of intersection for the value of altitude with the highest number of points. The area of intersection is made up of all the coordinates in that altitude level, as shown in Fig. 4.2b.

With all the information regarding the area of intersection stored, we arrive at the step where we need to calculate the waypoints for the different trajectories, as presented in Chapter 3. Matplotlib was once again used to facilitate the visualization of the trajectories presented in Fig. 4.3. Then, the selection of the trajectory is made, by adding the distance between points for each trajectory and selecting the one with the greatest distance. Taking into consideration the three examples depicted in Fig. 4.3, the selected trajectory would be trajectory 3, as it presents the greatest distance. This trajectory is presented in Fig. 4.4.

Depending on the length of the trajectory, the SNR margin may be considered. For that purpose, we simply put three **if** statements to increase the SNR needed for each FAP. The rationale for each **if** statement is explained in Algorithm 1. If a condition for one of the **if** statements is true,

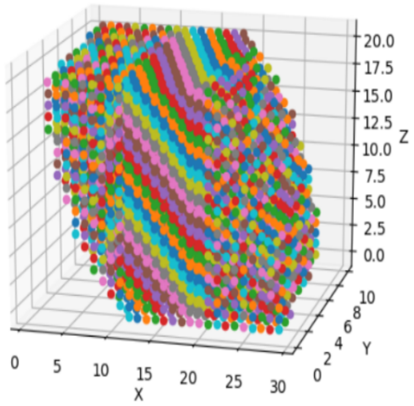

(a) Volume of intersection between two FAPs.

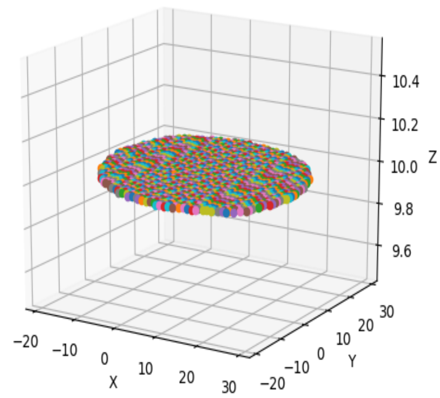

(b) Area of intersection between two FAPs

Figure 4.2: Different intersections between two FAPs.

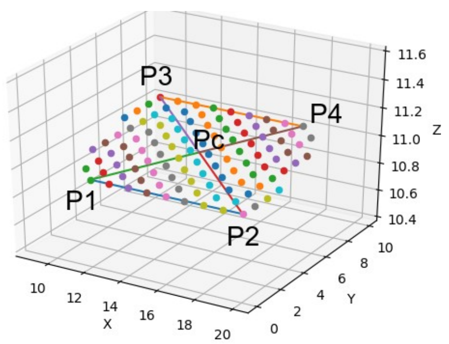

(a) Trajectory 1.

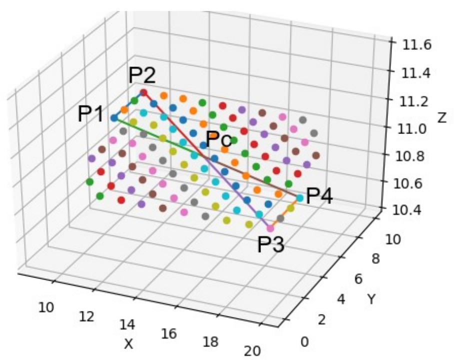

(b) Trajectory 2.

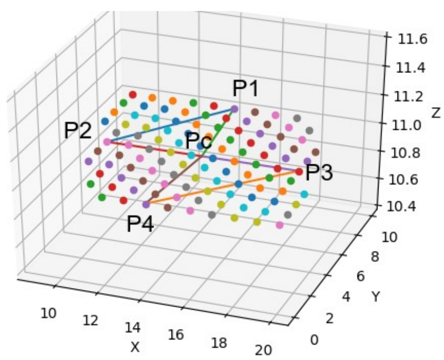

(c) Trajectory 3.

Figure 4.3: Trajectory examples.

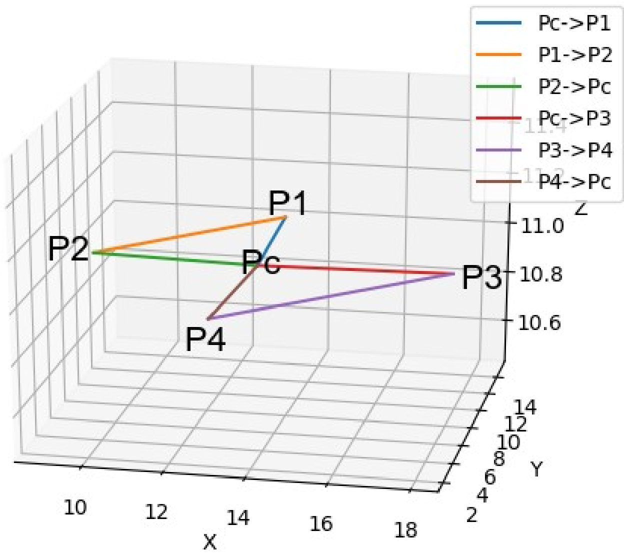

Figure 4.4: Selected trajectory, which is the one with the greatest distance, thus allowing to minimize the power consumption.

then the SNR is increased, and the *calculateValidPoints* function is executed again. After the area of intersection is recalculated, the waypoint definition is repeated and a new trajectory is selected.

Finally, the energy consumption to complete the selected trajectory is determined. For that purpose, we consider (4.1).

$$P(V) = P_b\left(1+\frac{3V^2}{U_{tip}^2}\right)+P_{ind}\left(\sqrt{1+\frac{V^4}{4v_0^4}}-\frac{V^2}{2v_0^2}\right)^{3/2}+\frac{1}{2}d_0\rho sAV^3 \tag{4.1}$$

To perform the calculations based on (4.1), a function named P was built, which takes as argument the velocity at which the GW UAV will perform the trajectory; it is presented in the following.

```
def P(V):
firstElement= P0*(1+(3*math.pow(V,2)/(math.pow(Utip,2))))
square=1+(math.pow(V,4)/(4*math.pow(V0,4)))
secondElement=Pi*math.pow((math.sqrt(square)-(math.pow(V,2)
    /(2*math.pow(V0,2)))),1/2)
thirdElement=(1/2)*d0*rho*s*A*math.pow(V,3)
return firstElement+secondElement+thirdElement
```

Each "*element*" in function P corresponds to an addend of Eq. 4.1. To get the velocity for the argument P, we need to calculate the value V that will minimize the return value; for that purpose, the *optimize* method from the SciPy [23] package was used.

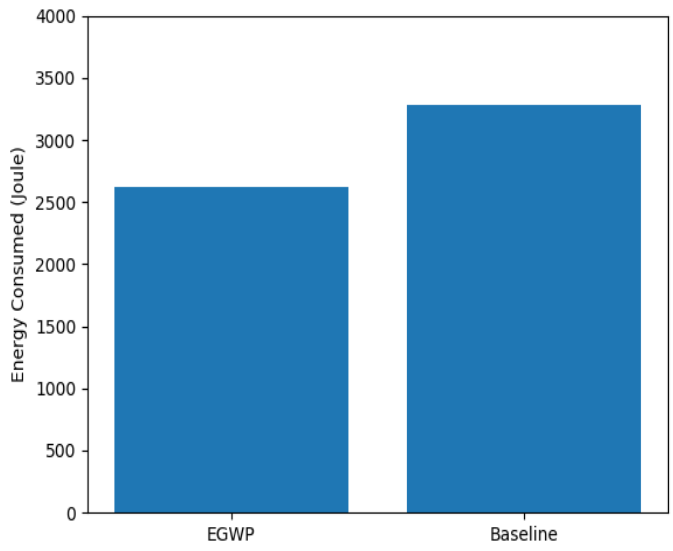

Figure 4.5: Graphical results provided by UAVPowerSim for energy consumption.

4.3 UAV Power Simulator Output

The output of UAVPowerSim consists of the velocity, V, and the power needed to complete the trajectory. To plot the difference in energy consumed for hovering and using the EGWP algorithm, we employed Matplotlib. An example of the graphical results provided by UAVPowerSim is presented in Fig. 4.5 and Fig. 4.6, whereas the detailed numerical results are provided in the terminal, as shown in Fig. 4.7.

4.4 Summary

In this chapter, the implementation of the UAVPowerSim was described. We started by explaining the input parameters related to the physical attributes of the UAV and the environment constants, which are necessary to calculate the energy consumption of the UAV. Then, the inputs necessary to apply the FSPL model were introduced, followed by the positions of the FAPs.

After the explanation of the initial setup, the implementation of the algorithm was detailed, starting with the function that calculates the area of intersection and the arguments it takes. The python packages necessary to execute the simulator were mentioned, and their usage was explained. The function developed to calculate the energy necessary to complete the trajectory was also described. Lastly, the outputs for the final results provided by UAVPowerSim were shown; they are composed of 1) two figures that show the total operational time of the UAV and its energy consumption in comparison with a baseline (hovering); and 2) the terminal output of the UAVPowerSim, which provides more detailed results than the figures.

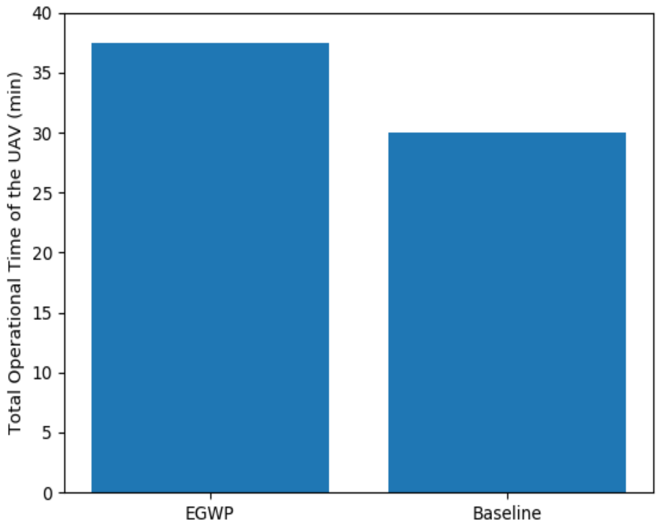

Figure 4.6: Graphical results provided by UAVPowerSim for operational time.

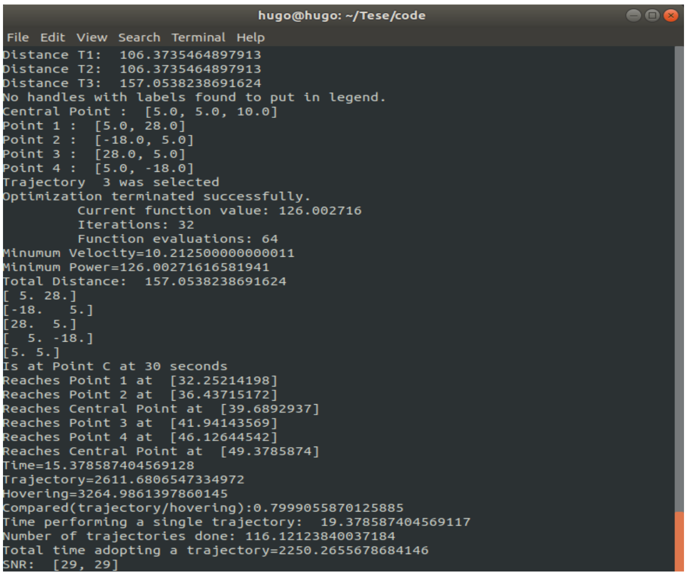

Figure 4.7: UAVPowerSim terminal output.

Chapter 5

Solution Evaluation

This chapter presents the energy consumption and network performance evaluation when employing the EGWP algorithm against the baseline, which considers the GW UAV in the hovering state. The evaluation metrics are described, and the performed evaluation is explained. The results are then analyzed, and the main conclusions are pointed out.

5.1 Evaluation Conditions

Due to the COVID-19 pandemic and the confinement rules recommended by the national authorities, which took place during the development of this dissertation, it was not possible to perform an experimental validation and evaluation of the EGWP algorithm using a real rotary-wing UAV. As a primary alternative, the Software In The Loop (SITL) simulator [24] was considered, since it allows to run the autopilot software and assess the behavior of a real UAV without any hardware, including the battery consumption over time. However, we quickly concluded that the battery consumption model in this simulator presents a linear behavior, which is not verified in real-world UAVs, as stated in the literature. For these reasons, the EGWP algorithm was evaluated by means of the UAVPowerSim simulator, from the energy consumption point of view, and using the ns-3 simulator, from the network performance point of view.

5.2 Energy Consumption and Network Performance Evaluation

In order to perform the energy consumption and network performance evaluation when employing the EGWP algorithm, some specific scenarios based on the general scenario presented in Chapter 3 and shown in Fig. 5.1 were defined, each with the aim of showing how the distance between the FAPs greatly influences the optimal positioning of the GW UAV. These scenarios were composed of a single GW UAV, and a variable number of FAPs, placed at different distances from each other: FAPs very close to each other; FAPs at a considerable distance from each other; FAPs positioned at the edge of the intersection between them; and FAPs randomly positioned. For traffic generation

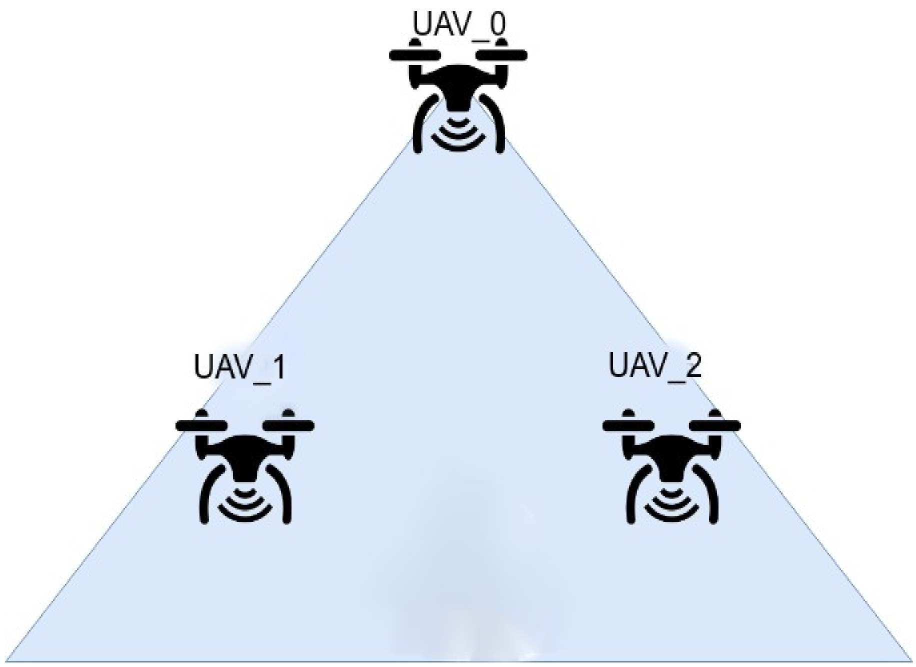

Figure 5.1: Reference scenario.

purposes, a maximum channel capacity of 500 Mbit/s was considered, which was divided by the number of FAPs sharing the medium, in order to define the traffic demand of each FAP.

The network performance evaluation took into account two QoS metrics: 1) aggregate throughput, which consists of the average number of bits received per second by the GW UAV; and 2) delay, which represents the time taken by each data packet to reach the sink application of the GW UAV, since the instant it was generated by the source application of each FAP, including queuing, transmission, and propagation delays; it was measured based on packets collected at each 10 ms, during the simulation time. First, the network performance evaluation was performed using only the FSPL model. Then, to perform a more realistic validation, Rician fast-fading was considered, by employing a realistic channel model built upon experimental results collected in an experimental testbed [25].

A more general evaluation of the EGWP algorithm was also performed, comparing average distances between a different number of FAPs to the gains obtained in the GW UAV lifetime. With this we were able to evaluate how a different number of FAPs and the distance between them affect the gains we can obtain in the GW UAV lifetime when employing the EGWP algorithm.

5.2.1 ns-3 Simulation Setup

To evaluate the network performance obtained with the EGWP algorithm, we used the ns-3 simulator. A Network Interface Card (NIC) was configured on each UAV in Ad Hoc mode, using the IEEE 802.11ac standard in channel 50, considering the parameters presented in Section 4.1. The traffic generated was UDP Poisson for a constant packet size of 1400 bytes. The data rate was automatically defined by the *MinstrelHtWifiManager* mechanism. The traffic generation was carried out during the 130 s simulation time. The Controlled Delay (CoDeL) algorithm [26], which is a queuing discipline that considers the time that packets are held in the transmission queue to discard packets, was used; this allows the mitigation of the bufferbloat problem. The default parameters of CoDeL [27] in ns-3 [28] were used. Regarding the network performance, the results are represented by the Cumulative Distribution Function (CDF) for the delay and by the complementary CDF (CCDF) for the aggregate throughput.

5.2.2 Evaluation Under Typical Networking Scenarios

In the following, we present the results obtained for the scenarios that were used to evaluate the EGWP algorithm. The particular scenarios used for the evaluation are based on the reference scenario shown in Fig. 5.1 and previously explained. We start by evaluating for scenarios where there are only 2 FAPs in the network, then we proceed to scenarios with 5 FAPs, lastly the evaluation was performed in scenarios with 10 FAPs. As previously mentioned, for a fixed number of FAPs we considered three different scenarios: FAPs very close to each other; FAPs at a considerable distance from each other; and FAPs positioned at the edge of the intersection between them.

5.2.2.1 2 FAPs

Firstly, we consider a scenario with two FAPs close to each other: one hovering at $(x_1, y_1, z_1) = (0, 0, 10)$ and the other at $(x_2, y_2, z_2) = (1, 0, 10)$. In order to enable an equidistant intersection area between the two FAPs, they were generating the same amount of traffic, which was set to 250 Mbit/s. The third trajectory was chosen, since its length is much longer than the other two (trajectory 1 is 122 m long, trajectory 2 is also 122 m long, while trajectory 3 is 196 m long), thus allowing to achieve a higher gain in the GW UAV lifetime. Each lap from this trajectory takes a total of $\approx$ 23 s to be completed, which enables 98 laps during the GW UAV lifetime, amounting to a total lifetime for the GW UAV of $\approx$ 38 min. To complete a lap, a total of $\approx$ 3096 J is consumed, while in hovering, a total of 3913 J is consumed, as depicted in Fig. 5.2a. This represents a gain in the total lifetime of the GW UAV of 26%, which is presented in Fig. 5.2b. The results for this scenario are shown in Fig. 5.3. For the aggregate throughput, the results show a decrease of 7% for the 90$^{\text{th}}$ percentile and 2% for the 50$^{\text{th}}$ percentile (c.f. Fig. 5.3a). For the delay, it is shown an increase of 20% for the 90$^{\text{th}}$ percentile and 123% for the 50$^{\text{th}}$ percentile (c.f. Fig. 5.3b). The last evaluation performed for this scenario added Rician fast-fading to the FSPL model; the results are shown in Fig. 5.4. The 50$^{\text{th}}$ percentile results show a decrease of 11% for the aggregate throughput, while an increase of 500% for the delay.

The second scenario represents two FAPs positioned at a considerable distance from each other; they were hovering at $(x_1, y_1, z_1) = (0, 0, 10)$ and $(x_2, y_2, z_2) = (29, 0, 10)$. We once again considered two FAPs generating the same amount of traffic, 250 Mbit/s, so the evaluation was focused on variations on distance and not variations on the traffic demand. The trajectory selected

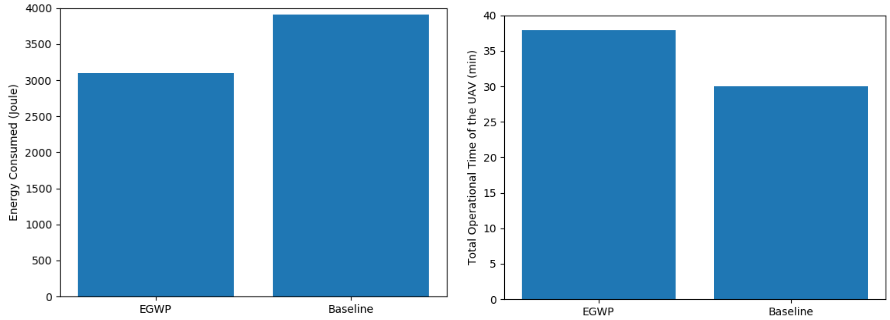

(a) Energy consumed by the GW UAV. (b) GW UAV lifetime.

Figure 5.2: Energy consumption results for 2 FAPs positioned close to each other.

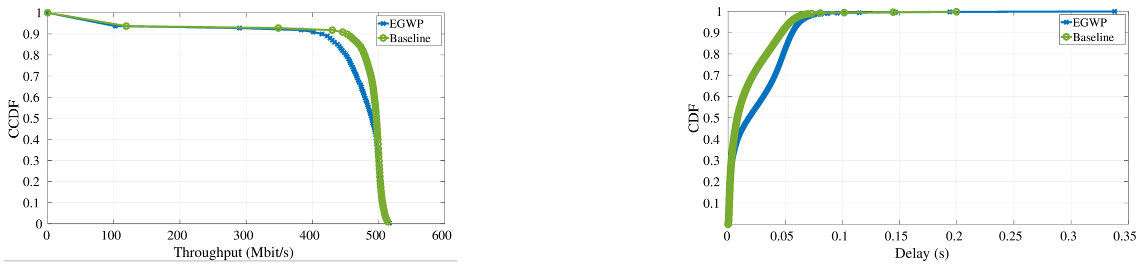

(a) Throughput. (b) Delay.

Figure 5.3: Network performance results, considering the FSPL model, for 2 FAPs positioned close to each other.

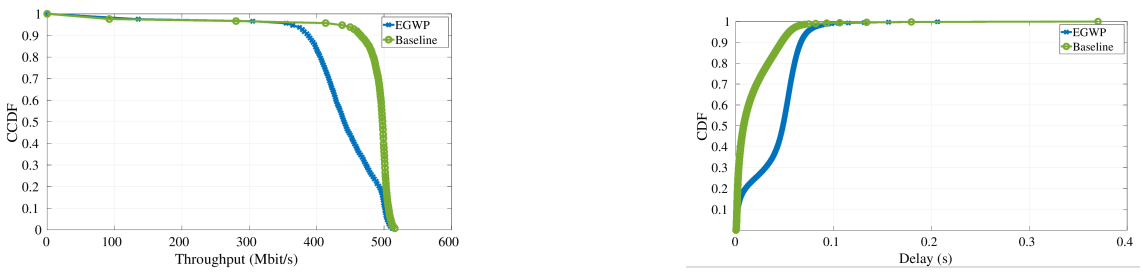

(a) Throughput. (b) Delay.

Figure 5.4: Network performance results, considering the Rician fast-fading component, for 2 FAPs positioned close to each other.

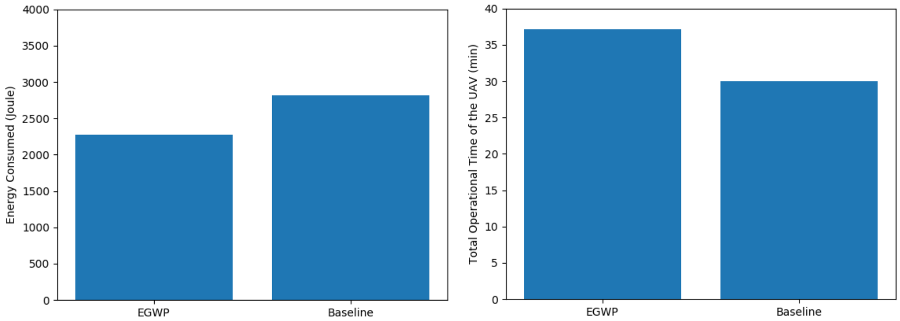

(a) Energy consumed by the GW UAV.

(b) GW UAV lifetime.

Figure 5.5: Energy consumption results for 2 FAPs positioned at a considerable distance from each other.

is also the third, as it presents greater length than the rest (trajectory 1 is 84 m long, trajectory 2 is 40.4 m long, and trajectory 3 is 105.7 m long). Each lap of this trajectory takes a total of $\approx$ 14 s to be completed, which enables 153 laps during the GW UAV lifetime, amounting to a total lifetime of $\approx$ 37 min. To complete a lap, a total of 1978 J is consumed, while hovering a total of $\approx$ 2418 J is consumed, as depicted in Fig. 5.5a. This represents a gain in the lifetime of the GW UAV of 22%, as presented in Fig. 5.5b. The network performance results only considering FSPL for this scenario are shown in Fig. 5.6, where the results show a decrease in aggregate throughput of 9% for the 90$^{\text{th}}$ percentile and 3% for the 50$^{\text{th}}$ percentile (c.f. Fig. 5.6a). For the delay, it is shown an increase of 30% for the 90$^{\text{th}}$ percentile and 214% for the 50$^{\text{th}}$ percentile, (c.f. Fig. 5.6b). The last evaluation performed for this scenario added Rician fast-fading to the FSPL model; the results are shown in Fig. 5.7. The 50$^{\text{th}}$ percentile results show a decrease of 10% for the aggregate throughput, while an increase of 941% for the delay.

It is observable a relevant degradation in the network performance when employing the EGWP algorithm in this scenario; so, as presented in Chapter 3, a SNR margin was added to the EGWP algorithm. The results are shown in Fig. 5.8, and it is possible to observe that we can achieve results closer to those obtained when the GW UAV is hovering. This happens because we are limiting the area within which the GW UAV can move, by drawing a smaller area inside the initial area, in order the GW UAV does not go as far from the FAPs as it was capable if the whole intersection area was considered.

The third scenario consists of two FAPs placed at a great distance from each other, which significantly reduces the area of intersection between them. For that purpose, they were hovering at positions $(x_1, y_1, z_1) = (0, 0, 10)$ and $(x_2, y_2, z_2) = (58, 0, 10)$. The FAPs were generating the same amount of traffic: 250 Mbit/s. In this scenario, the second trajectory was selected, as it presents greater length than the rest (trajectory 1 is 8 m long, trajectory 2 is 16 m long, and trajectory 3 is 8 m long). Each lap in this trajectory takes a total of $\approx$ 6 s to be completed, which enables a total of 348 laps during the GW UAV lifetime, amounting to a total of $\approx$ 32 min. To complete a lap, a total of $\approx$ 871 J is consumed, while in hovering a total of $\approx$ 937 J is consumed, as shown

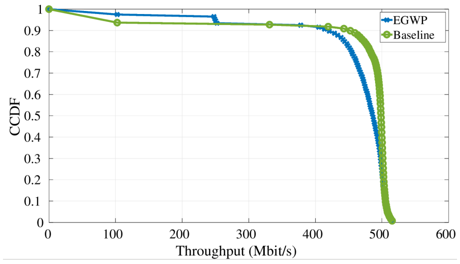

(a) Throughput.

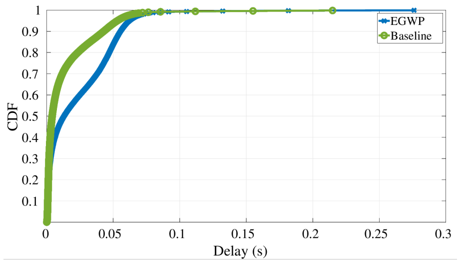

(b) Delay.

Figure 5.6: Network performance results, considering the FSPL model, for 2 FAPs positioned at a considerable distance from each other.

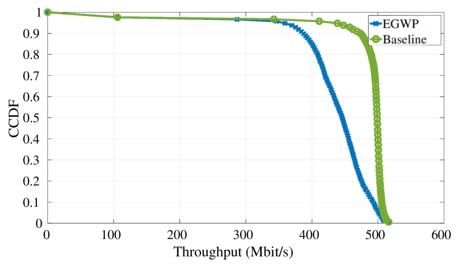

(a) Throughput.

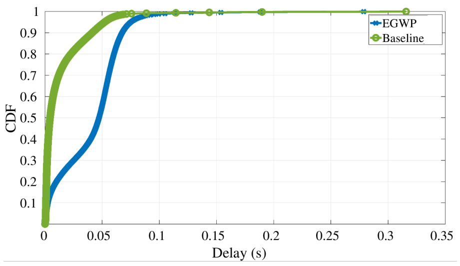

(b) Delay.

Figure 5.7: Network performance results, considering the Rician fast-fading component, for 2 FAPs positioned at a considerable distance from each other.

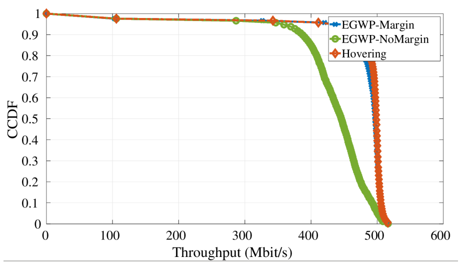

(a) Throughput.

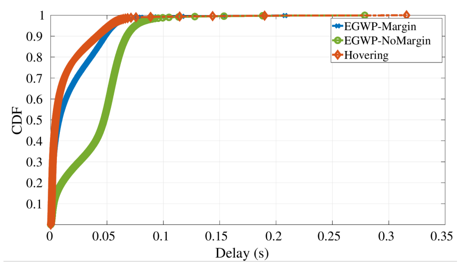

(b) Delay.

Figure 5.8: Performance results considering the EGWP with and without SNR margin, complemented with results for hovering, for 2 FAPs positioned at a considerable distance from each other.

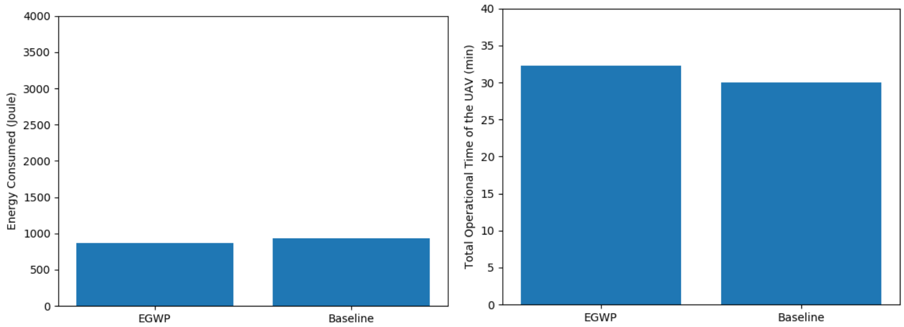

(a) Energy consumed by the GW UAV. (b) GW UAV lifetime.

Figure 5.9: Energy consumption results for 2 FAPs positioned at a great distance from each other.

in Fig. 5.9a. This represents a gain in the total lifetime of the GW UAV of 7%, as presented in Fig. 5.9b. For the aggregate throughput, the results show a decrease of 2% for the 90$^{\text{th}}$ percentile and 2% for the 50$^{\text{th}}$ percentile (c.f. Fig. 5.10a). For the delay, it is shown a decrease of 1% for the 90$^{\text{th}}$ percentile and 1% for the 50$^{\text{th}}$ percentile (c.f. Fig. 5.10b). Hence, the QoS degradation is negligible. The last evaluation performed for this scenario added Rician fast-fading to the FSPL model; the results are shown in Fig. 5.11. The 50$^{\text{th}}$ percentile results show an increase of 1% for the aggregate throughput, while a decrease of 1% for the delay.

5.2.2.2 5 FAPs

First, we considered the scenario composed of five FAPs close to each other, which were hovering at $(x_1, y_1, z_1) = (19, 40, 12)$, $(x_2, y_2, z_2) = (1, 0, 10)$, $(x_3, y_3, z_3) = (7, 17, 17)$, $(x_4, y_4, z_4) = (9, 16, 7)$, and $(x_5, y_5, z_5) = (10, 36, 13)$. They were generating the same amount of traffic, which was set to 100 Mbit/s. The second trajectory was chosen, since its length is superior to the other two (trajectory 1 is 55 m long, trajectory 2 is 74 m long, and trajectory 3 is 66 m long), thus allowing to achieve a higher gain in the GW UAV lifetime. Each lap of this trajectory takes a total of $\approx$ 11 s to be completed, which enables 191 laps during the GW UAV lifetime, amounting to a total lifetime of the GW UAV of $\approx$ 36 min. A total of $\approx$ 1584 J is consumed to complete a lap, while in hovering

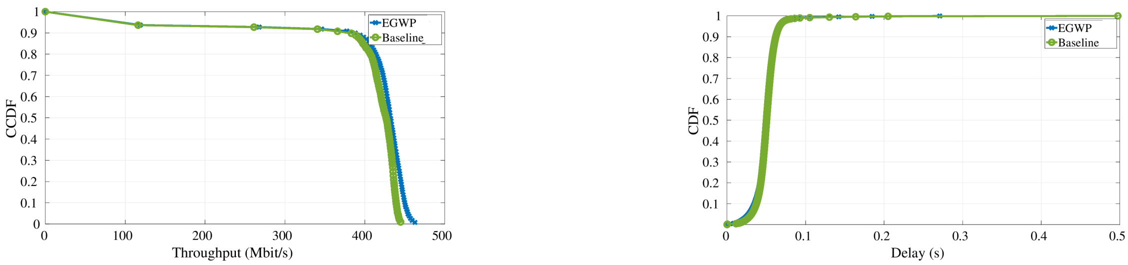

(a) Throughput. (b) Delay.

Figure 5.10: Network performance results, considering the FSPL model, for 2 FAPs positioned at a great distance from each other.

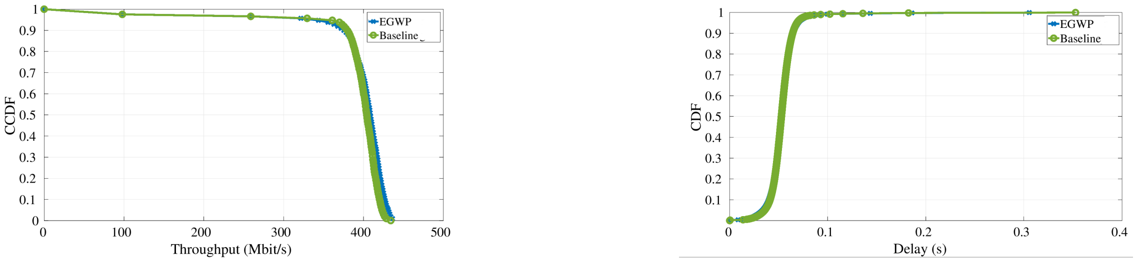

(a) Throughput. (b) Delay.

Figure 5.11: Network performance results, considering the Rician fast-fading component, for 2 FAPs positioned at a great distance from each other.

a total of 1890 J is consumed, as depicted in Fig. 5.12a. This represents a gain in the total lifetime of the GW UAV of 19%, presented in Fig. 5.12b. The results for this scenario using the FSPL model are shown in Fig. 5.13, where the results for the aggregate throughput show an increase of 1% for the 90$^{\text{th}}$ percentile and a decrease of 1% for the 50$^{\text{th}}$ percentile (c.f. Fig. 5.13a). For the delay, it is shown an increase of 5% for the 90$^{\text{th}}$ percentile and 4% for the 50$^{\text{th}}$ percentile (c.f. Fig. 5.13b). The last evaluation performed for this scenario added Rician fast-fading to the FSPL model; the results are shown in Fig. 5.14. It is observable a degradation lower than 7% for all the QoS metrics. The 50$^{\text{th}}$ percentile results show a decrease of 6% for the aggregate throughput, while an increase of 4% for the delay.

Then, we considered the scenario with five FAPs hovering at $(x_1,y_1,z_1) = (40,38,12)$, $(x_2,y_2,z_2) = (4,23,3)$, $(x_3,y_3,z_3) = (13,29,6)$, $(x_4,y_4,z_4) = (27,3,4)$, and $(x_5,y_5,z_5) = (18,42,18)$. The FAPs were generating 100 Mbit/s of traffic each. The trajectory selected was the third, as it presents greater length than the rest (trajectory 1 is 46 m long, trajectory 2 is 50 m long, and trajectory 3 is 55 m long). Each lap of this trajectory takes a total of ≈ 9 s to be completed, which enables 224 laps during the GW UAV lifetime, amounting to a total lifetime of ≈ 35 min. A total of 1349 J is consumed to complete a lap, while in hovering a total of ≈ 1577 J is consumed, as depicted in Fig. 5.15a. This represents a gain in the lifetime of the GW UAV of 16%, as presented in Fig. 5.15b.

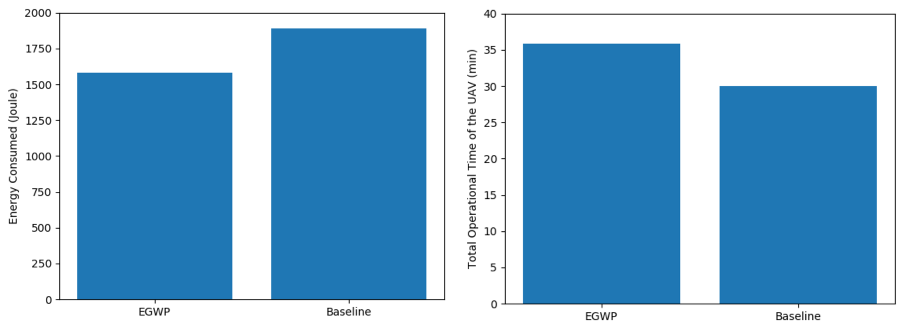

(a) Energy consumed by the GW UAV. (b) GW UAV lifetime.

Figure 5.12: Energy consumption results for 5 FAPs positioned close to each other.

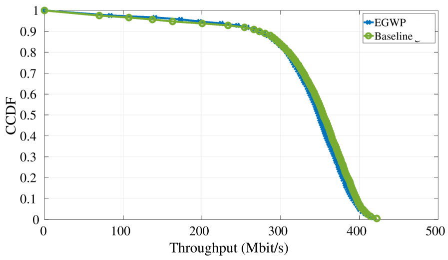

(a) Throughput.

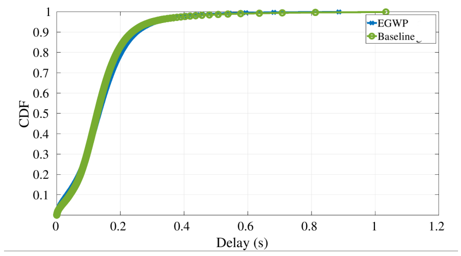

(b) Delay.

Figure 5.13: Network performance results, considering the FSPL model, for 5 FAPs positioned close to each other.

The network performance results only considering FSPL for this case are shown in Fig. 5.16. For the aggregate throughput, the results show a decrease of 5% for the 90$^{\text{th}}$ percentile and 5% for the 50$^{\text{th}}$ percentile (c.f. Fig. 5.7a). For the delay, it is shown an increase of 6% for the 90$^{\text{th}}$ percentile and 10% for the 50$^{\text{th}}$ percentile (c.f. Fig. 5.7b). The last evaluation performed for this scenario added Rician fast-fading to the FSPL model; the results are shown in Fig. 5.17. It is observable a negligible degradation in all the QoS metrics. The 50$^{\text{th}}$ percentile results show a decrease of 4% for the aggregate throughput, while an increase of 6% for the delay.

Lastly, the scenario with five FAPs placed at a great distance from each other was considered; the FAPs were hovering at $(x_1, y_1, z_1) = (30, 32, 2)$, $(x_2, y_2, z_2) = (3, 45, 0)$, $(x_3, y_3, z_3) = (43, 4, 6)$, $(x_4, y_4, z_4) = (23, 3, 7)$, and $(x_5, y_5, z_5) = (2, 16, 15)$, and generating 100 Mbit/s of traffic each. For this scenario, the second trajectory was selected, although trajectory 1 has the same length, so either could be chosen (trajectory 1 is 8 m long, trajectory 2 is 8 m long, and trajectory 3 is 0 m long). Each lap of this trajectory takes a total of $\approx$ 5 s to be completed, which enables a total of 389 laps during the GW UAV lifetime, amounting to a total of $\approx$ 31 min. A total of $\approx$ 778 J is consumed to complete a lap, while in hovering a total of $\approx$ 814 J is consumed, as shown in Fig. 5.18a. This represents a gain in the total lifetime of the GW UAV of 4%, as presented in Fig. 5.18b. The network performance results only considering FSPL for this scenario are shown in Fig. 5.19. For the aggregate throughput, the results show a decrease of 1% for the 90$^{\text{th}}$ percentile and

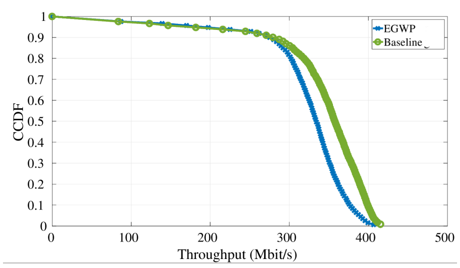

(a) Throughput.

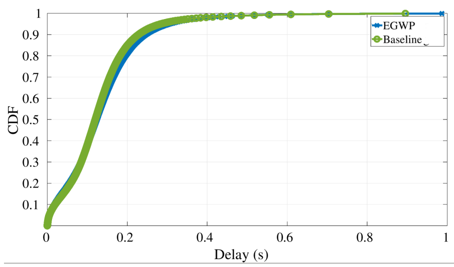

(b) Delay.

Figure 5.14: Network performance results, considering the Rician fast-fading component, for 5 FAPs positioned close to each other.

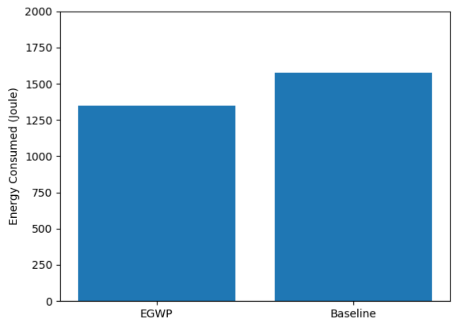

(a) Energy consumed by the GW UAV.

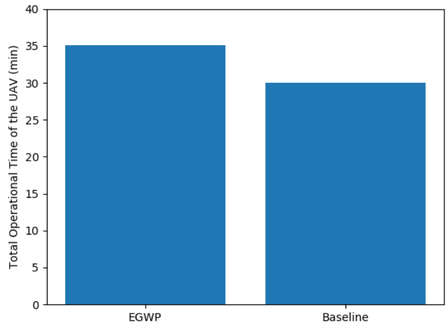

(b) GW UAV lifetime.

Figure 5.15: Energy consumption results for 5 FAPs positioned at a considerable distance from each other.

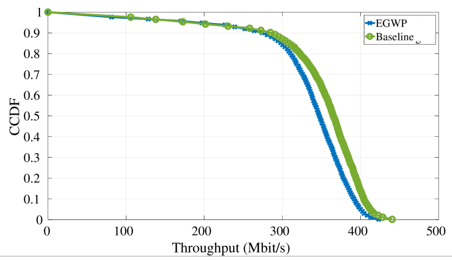

(a) Throughput.

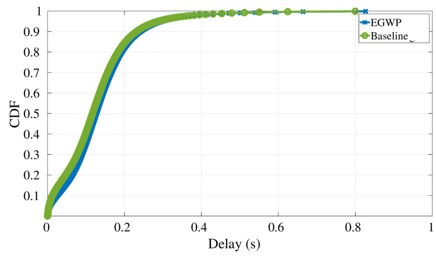

(b) Delay.

Figure 5.16: Network performance results, considering the FSPL model, for 5 FAPs positioned at a considerable distance from each other.

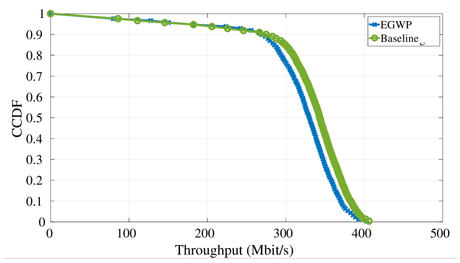

(a) Throughput.

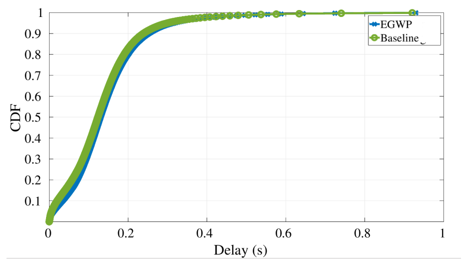

(b) Delay.

Figure 5.17: Network performance results, considering the Rician fast-fading component, for 5 FAPs positioned at a considerable distance from each other.

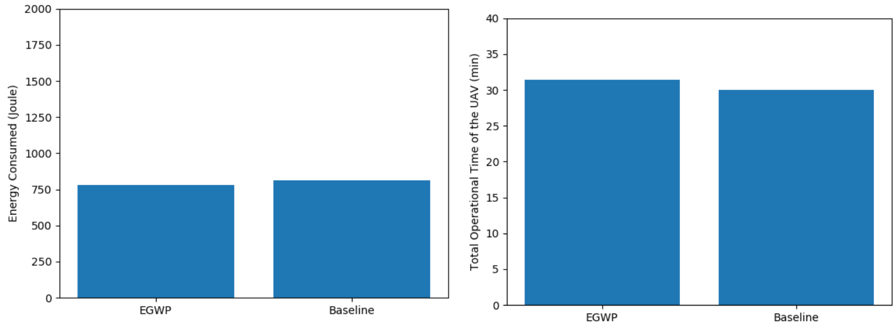

(a) Energy consumed by the GW UAV. (b) GW UAV lifetime.

Figure 5.18: Energy consumption results for 5 FAPs positioned at a great distance from each other.

1% for the 50th percentile (c.f. Fig. 5.19a). Lastly, for the delay, it is shown an increase of 2% for the 90th percentile and 4% for the 50th percentile (c.f. Fig. 5.19b). The last evaluation performed for this scenario added Rician fast-fading to the FSPL model; the results are shown in Fig. 5.20. The 50th percentile shows a decrease of 2% for the aggregate throughput, while an increase of 4% for the delay.

5.2.2.3 10 FAPs

First, we considered the scenario with ten FAPs close to each other, which were hovering at $(x_1,y_1,z_1) = (20,25,18)$, $(x_2,y_2,z_2) = (9,20,17)$, $(x_3,y_3,z_3) = (20,13,5)$, $(x_4,y_4,z_4) = (24,35,13)$, $(x_5,y_5,z_5) = (20,40,7)$, $(x_6,y_6,z_6) = (35,42,12)$, $(x_7,y_7,z_7) = (41,30,15)$, $(x_8,y_8,z_8) = (40,25,1)$, $(x_9,y_9,z_9) = (14,43,17)$, and $(x_{10},y_{10},z_{10}) = (29,19,13)$. They were generating the same amount of traffic, which was set to 50 Mbit/s. The third trajectory was chosen, since its length is superior to the other two (trajectory 1 is 61 m long, trajectory 2 is 56 m long, and trajectory 3 is 79 m long). Each lap of this trajectory takes a total of $\approx$ 12 s to be completed, which enables 185 laps during the GW UAV lifetime, amounting to a total lifetime of the GW UAV of $\approx$ 36 min. To complete a lap a total of $\approx$ 1643 J is consumed, while in hovering a total of 1969 J is consumed, as depicted in Fig. 5.21a. This represents a gain in the total lifetime of the GW UAV of 20%, which is presented

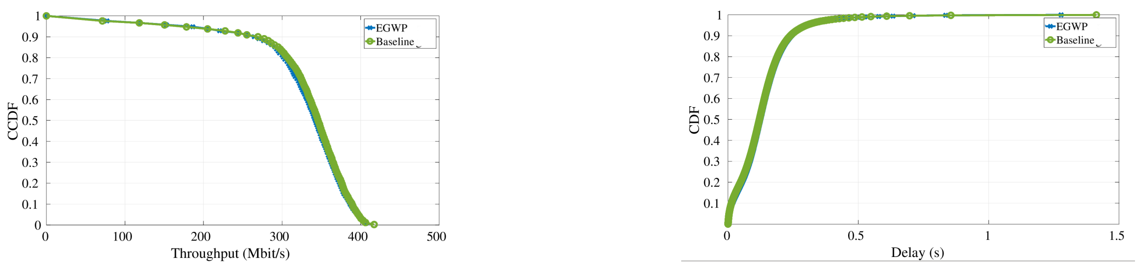

(a) Throughput. (b) Delay.

Figure 5.19: Network performance results, considering the FSPL model, for 5 FAPs positioned at a great distance from each other.

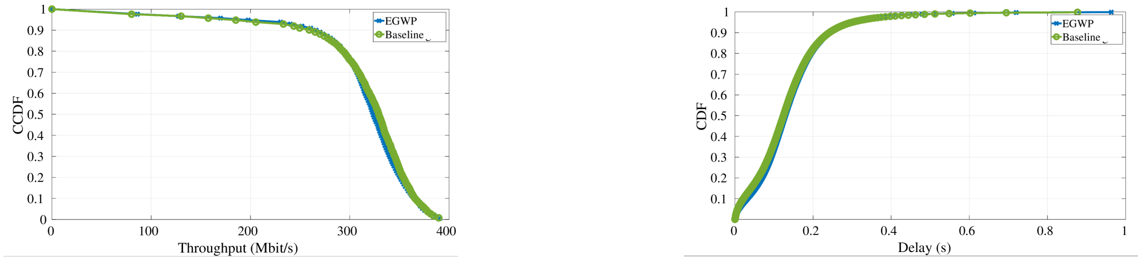

(a) Throughput. (b) Delay.

Figure 5.20: Network performance results, considering the Rician fast-fading component, for 5 FAPs positioned at a great distance from each other.

in Fig. 5.21b. The results for this scenario, considering FSPL, are shown in Fig. 5.22. For the aggregate throughput, the results show a decrease of 2% for the 90th percentile and 1% for the 50th percentile (c.f. Fig. 5.22a). For the delay, it is shown an increase of 5% for the 90th percentile and 5% for the 50th percentile (c.f. Fig. 5.22b). The last evaluation performed for this scenario added Rician fast-fading to the FSPL model; the results are shown in Fig. 5.23. It is observable negligible degradation in all the QoS metrics. The 50th percentile results show a decrease of 2% for the aggregate throughput, while an increase of 2% for the delay.

The second scenario was composed of ten FAPs hovering at $(x_1,y_1,z_1) = (41,31,13)$, $(x_2,y_2,z_2) = (39,3,0)$, $(x_3,y_3,z_3) = (17,30,4)$, $(x_4,y_4,z_4) = (20,20,1)$, $(x_5,y_5,z_5) = (12,49,7)$, $(x_6,y_6,z_6) = (38,23,10)$, $(x_7,y_7,z_7) = (33,24,18)$, $(x_8,y_8,z_8) = (25,38,9)$, $(x_9,y_9,z_9) = (36,20,19)$, and $(x_{10}, y_{10},z_{10}) = (39,24,17)$. We once again considered ten FAPs generating the same amount of traffic: 50 Mbit/s. The trajectory selected was the first, as it presents greater length than the rest (trajectory 1 is 40 m long, trajectory 2 is 39 m long, and trajectory 3 is 19 m long). Each lap of this trajectory takes a total of $\approx$ 8 s to be completed, which enables 260 laps during the GW UAV lifetime, amounting to a total lifetime of $\approx$ 34 min. To complete a lap, a total of 1167 J is consumed, while in hovering a total of $\approx$ 1333 J is consumed, as depicted in Fig. 5.24a. This represents a gain in the lifetime of the GW UAV of 14%, as presented in Fig. 5.24b. The network performance results for

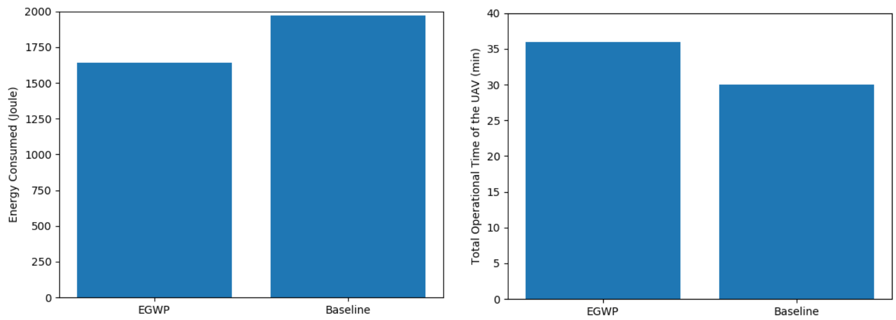

(a) Energy consumed by the GW UAV. (b) GW UAV lifetime.

Figure 5.21: Energy consumption results for 10 FAPs positioned close to each other.

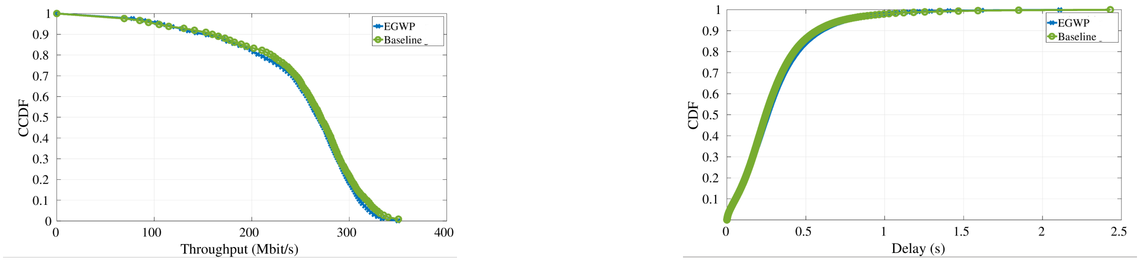

(a) Throughput. (b) Delay.

Figure 5.22: Network performance results, considering the FSPL model, for 10 FAPs positioned close to each other.

this scenario, considering FSPL, are shown in Fig. 5.25. For the aggregate throughput, the results show an increase of 2% for the 90$^{\text{th}}$ percentile and a decrease of 3% for the 50$^{\text{th}}$ percentile (c.f. Fig. 5.25a). For the delay, it is shown a decrease of 0.29% for the 90$^{\text{th}}$ percentile and an increase of 4% for the 50$^{\text{th}}$ percentile (c.f. Fig. 5.25b). The last evaluation performed for this scenario added Rician fast-fading to the FSPL model; the results are shown in Fig. 5.26. It is observable negligible degradation in all the QoS metrics. The 50$^{\text{th}}$ percentile results show a decrease of 2% for the aggregate throughput, and an increase of 2% for the delay.

Lastly, the scenario with 10 FAPs placed at a great distance from each other, hovering at $(x_1, y_1, z_1) = (41, 48, 14)$, $(x_2, y_2, z_2) = (44, 3, 15)$, $(x_3, y_3, z_3) = (16, 4, 3)$, $(x_4, y_4, z_4) = (11, 9, 2)$, $(x_5, y_5, z_5) = (40, 36, 5)$, $(x_6, y_6, z_6) = (24, 35, 15)$, $(x_7, y_7, z_7) = (29, 40, 8)$, $(x_8, y_8, z_8) = (46, 32, 14)$, $(x_9, y_9, z_9) = (3, 11, 16)$, and $(x_{10}, y_{10}, z_{10}) = (25, 27, 6)$. The FAPs were generating 50 Mbit/s of traffic each. For this scenario, the third trajectory was selected (trajectory 1 is 9 m long, trajectory 2 is 10 m long, and trajectory 3 is 10.2 m long). Each lap of this trajectory takes a total of ≈ 5 s to be completed, which enables a total of 379 laps during the GW UAV lifetime, amounting to a total of ≈ 32 min. A total of ≈ 800 J is consumed to complete a lap, while in hovering a total of ≈ 843 J is consumed, as shown in Fig. 5.27a. This represents a gain in the total lifetime of the GW UAV of 5%, as presented in Fig. 5.27b. The network performance results only considering FSPL for this scenario are shown in Fig. 5.28. For the aggregate throughput, the results show a

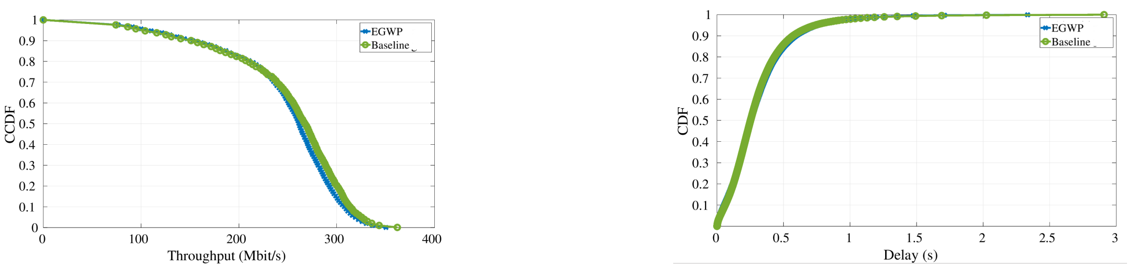

(a) Throughput. (b) Delay.

Figure 5.23: Network performance results, considering the Rician fast-fading component, for 10 FAPs positioned close to each other.

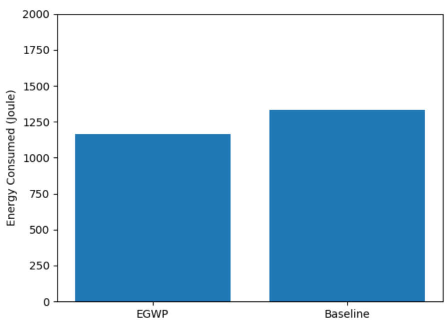

(a) Energy consumed by the GW UAV.

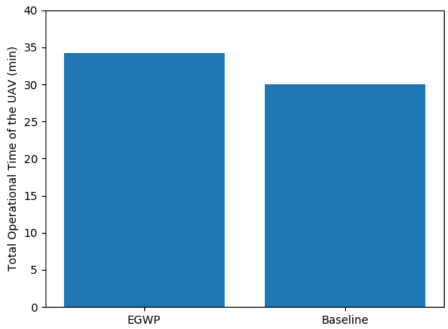

(b) GW UAV lifetime.

Figure 5.24: Energy consumption results for 10 FAPs positioned at a considerable distance from each other.

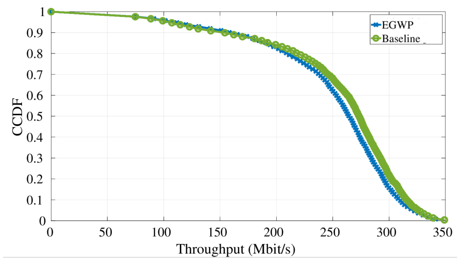

(a) Throughput.

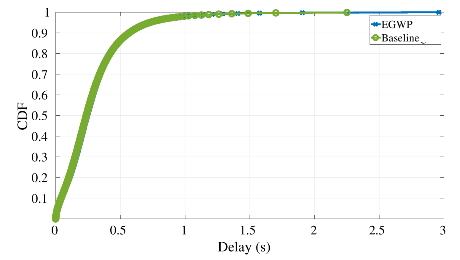

(b) Delay.

Figure 5.25: Network performance results, considering the FSPL model, for 10 FAPs positioned at a considerable distance from each other.

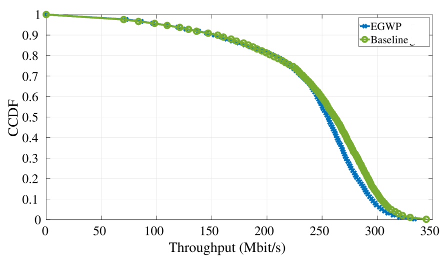

(a) Throughput.

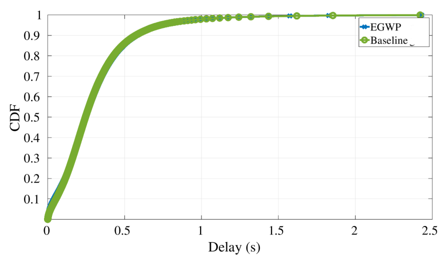

(b) Delay.

Figure 5.26: Network performance results, considering the FSPL model, for 10 FAPs positioned at a considerable distance from each other.

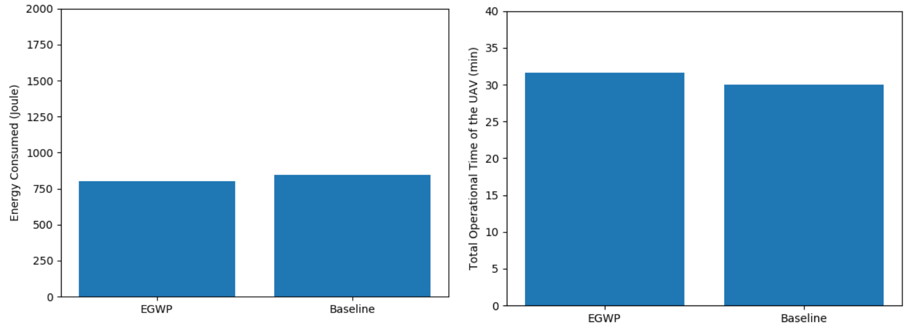

(a) Energy consumed by the GW UAV.

(b) GW UAV lifetime.

Figure 5.27: Network performance results considering the FSPL model, for 10 FAPs positioned at a great distance from each other.

decrease of 5% for the 90$^{\text{th}}$ percentile and 3% for the 50$^{\text{th}}$ percentile (c.f. Fig. 5.28a). For the delay, it is shown an increase of 3% for the 90$^{\text{th}}$ percentile and 4% for the 50$^{\text{th}}$ percentile (c.f. Fig. 5.28b). The last evaluation performed for this scenario added Rician fast-fading to the FSPL model; the results are shown in Fig. 5.29. The 50$^{\text{th}}$ percentile results show an increase of 2% for the aggregate throughput, while a decrease of 5% for the delay.

5.2.3 Evaluation Under Random Networking Scenarios

After the validation of the EGWP algorithm under typical networking scenarios, the evaluation of the EGWP algorithm from the energy consumption point of view under random networking scenarios was performed. With this in mind, the evaluation of how different numbers of FAPs and the average distance between FAPs influences the gains obtained by the EGWP algorithm is shown in Fig. 5.30. The results are shown in Fig. 5.30 were obtained from a set of 160 networking scenarios, considering a different number of FAPs. The scenarios were generated using BonnMotion [29], which is a mobility scenario generation tool. In the simulations for the same number of FAPs, all the FAPs were generating the same amount of traffic. It is possible to observe that the higher the distance between the FAPs, the lower the gains obtained using the

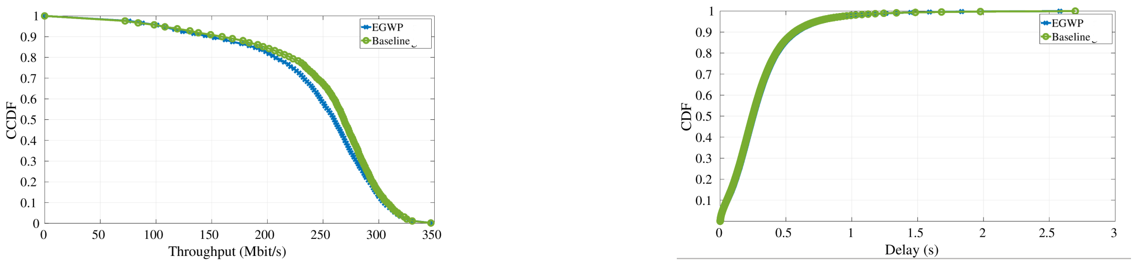

(a) Throughput.

(b) Delay.

Figure 5.28: Network performance results, considering the FSPL model, for 10 FAPs positioned at a great distance from each other.

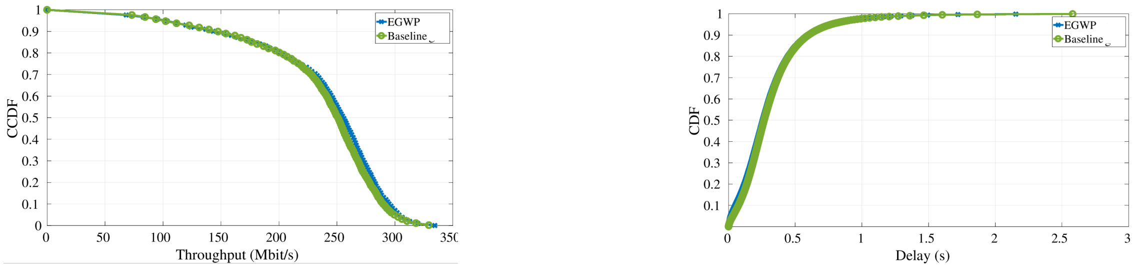

(a) Throughput.

(b) Delay.

Figure 5.29: Network performance results, considering the Rician fast-fading component, for 10 FAPs positioned at a great distance from each other.

EGWP algorithm, which is according to the results obtained for the typical networking scenarios. Another conclusion that can be drawn is that for equal average distance between the FAPs, the gains decrease when the number of FAPs increases; this is mainly due to the decrease in the size of the area of intersection that occurs as more FAPs are added.

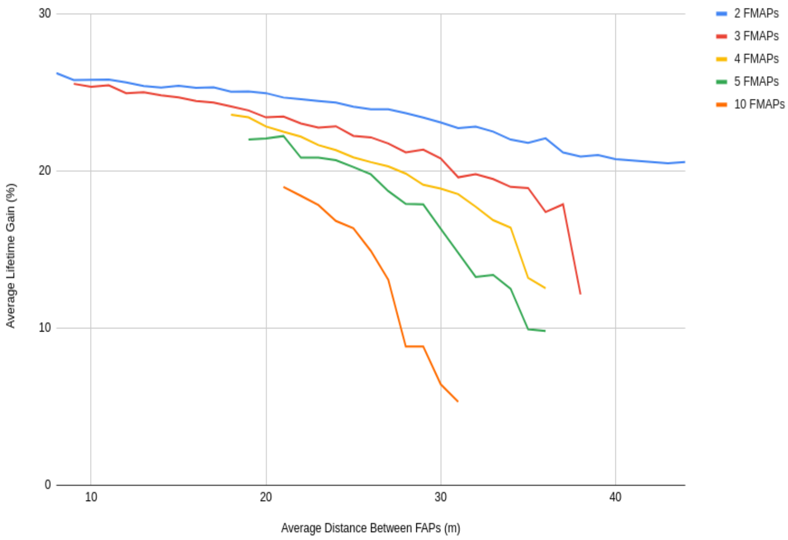

Figure 5.30: Impact of both the average distance between the FAPs and the number of FAPs on the gains in the GW UAV lifetime obtained.

5.3 Discussion

From the results shown in this chapter, it is possible to conclude that, regarding energy efficiency, the higher the number of FAPs in the network, the lower are the gains that we can obtain by using the EGWP algorithm; this is mainly due to the decrease in the area of intersection that occurs as the number of FAPs increases. For networking scenarios where the FAPs are close to each other, making that the distance between each FAP and the GW UAV increases more significantly than if the intersection area was smaller, the QoS performance is lower than in hovering. As the distance between each FAP and the GW UAV increases, the SNR of the wireless link decreases, the capacity of the wireless channel is reduced, and the packets are held in the transmission queues longer. Therefore, the throughput decreases, and the delay increases. For scenarios where the FAPs are at a considerable distance from each other, the results obtained are similar to the scenarios where the FAPs are close to each other. For scenarios where the FAPs are far away from each other, we conclude that there is no network performance degradation when employing the EGWP algorithm, compared to the baseline; this happens because the area of intersection is so small that the movement that the GW UAV performs during the trajectory is minimum. The same conclusion is applied when the number of FAPs on the network increases.

When employing Rician fast-fading, it is possible to achieve simulation results closer to the ones measured in the real world, since the random component added by Rician replicates some stochastic events and environment particularities that may degrade the performance of the network. As expected, the results achieved when employing the Rician fast-fading component show a clear degradation in the network performance with respect to the simulation environment that considers only the FSPL model. Similarly to what happens when only the FSPL model was considered, the scenarios for which the GW UAV has to perform an extensive movement to complete the trajectory tend to present worse results when compared to hovering. Taking into account this conclusion, a SNR margin was added to the EGWP algorithm to limit the area of intersection when the FAPs are in close proximity with each other. The results when applying the SNR margin clearly show an improvement in the network performance when compared to the EGWP algorithm without the SNR margin, and they are closer to the results obtained in hovering.

Chapter 6

Conclusions

FNs can play a significant role in providing broadband Internet access in temporary events. For that purpose, UAVs, which have high mobility and can carry cargo on board, are perfect platforms for carrying Wi-Fi Access Points and cellular Base Stations.

The positioning of the GW UAV, which is the node responsible for forwarding traffic to/from the Internet, can greatly affect the overall FN performance, especially if the FAPs have different traffic demands. However, as it was shown, this issue has been largely overlooked in the state of the art.

Another issue that should be taken into consideration when addressing FNs is the limited battery capacity of the UAV. Unlike ground-based networks, which are typically connected to the electrical grid, UAVs only rely on their battery capacity, which is heavily drained by the various movements performed by the UAV. In the literature, it is shown that the energy consumption for movement in rotary-wing UAVs does not have an uniform behavior: it decreases for low-velocity values, and then it starts increasing as velocity increases, which leads to the conclusion that hovering is not the most energy-efficient movement.

In this dissertation, an Energy-aware GateWay Positioning (EGWP) algorithm was proposed and implemented. EGWP takes into account the energy consumption of the GW UAV and the traffic demands of the FAPs to define the trajectory and speed of the GW UAV that minimize its energy consumption, while maintaining the QoS offered by the FN.

In order to evaluate the energy consumption of the GW UAV when employing the EGWP algorithm, a custom-tailored simulator was built, called UAVPowerSim. The evaluation regarding network performance when the EGWP algorithm is employed was evaluated by means of ns-3 simulations, focusing on two metrics: 1) aggregate throughput; and 2) delay. The EGWP evaluation carried out allowed to conclude that it is possible to increase the lifetime of the GW UAV without compromising the QoS offered by the FN.

In the end, the objectives of this dissertation were fully achieved. The main difficulties that occurred during this dissertation were caused by the COVID-19 pandemic, which made it impossible to perform an experimental evaluation of the EGWP algorithm using a real rotary-wing UAV.

With the lack of simulators with accurate battery consumption models for UAVs, we were not able to counter-validate the results obtained with UAVPowerSim.

As future work, there are some improvements to the EGWP algorithm and UAV Power Simulator developed in this dissertation that could be made:

- Experimental validation of the results obtained with UAVPowerSim.
- Experimental validation of the results obtained with ns-3.
- Study of additional trajectories that can be added to the EGWP algorithm.
- Development of an energy consumption model for circular movements performed by rotary-wing UAVs, based on experimental measurements.
- Evolve the EGWP algorithm to address the cases where there is no intersection between the spheres representing the communications range of the FAPs.

References

[1] Eduardo Nuno Almeida, Rui Campos, and Manuel Ricardo. Traffic-aware multi-tier flying network: Network planning for throughput improvement. In *2018 IEEE Wireless Communications and Networking Conference (WCNC)*, pages 1–6. IEEE, 2018.

[2] Yong Zeng, Rui Zhang, and Teng Joon Lim. Wireless communications with unmanned aerial vehicles: Opportunities and challenges. *IEEE Communications Magazine*, 54(5):36–42, 2016.

[3] André Coelho, Eduardo Nuno Almeida, Pedro Silva, José Ruela, Rui Campos, and Manuel Ricardo. Redefine: Centralized routing for high-capacity multi-hop flying networks. In *2018 14th International Conference on Wireless and Mobile Computing, Networking and Communications (WiMob)*, pages 75–82. IEEE, 2018.

[4] André Coelho, Rui Campos, and Manuel Ricardo. Traffic-aware gateway placement for high-capacity flying networks. *arXiv preprint arXiv:1912.09413*, 2019.

[5] Mohammad Mozaffari, Walid Saad, Mehdi Bennis, Young-Han Nam, and Mérouane Debbah. A tutorial on uavs for wireless networks: Applications, challenges, and open problems. *IEEE Communications Surveys & Tutorials*, 21(3):2334–2360, 2019.

[6] Yong Zeng, Jie Xu, and Rui Zhang. Energy minimization for wireless communication with rotary-wing uav. *IEEE Transactions on Wireless Communications*, 18(4):2329–2345, 2019.

[7] Shih-Fan Chou, Ai-Chun Pang, and Ya-Ju Yu. Energy-aware 3d unmanned aerial vehicle deployment for network throughput optimization. *IEEE Transactions on Wireless Communications*, 19(1):563–578, 2019.

[8] Erlend Larsen, Lars Landmark, and Øivind Kure. Optimal uav relay positions in multi-rate networks. In *2017 Wireless Days*, pages 8–14. IEEE, 2017.

[9] Qingqing Wu, Liang Liu, and Rui Zhang. Fundamental trade-offs in communication and trajectory design for uav-enabled wireless network. *IEEE Wireless Communications*, 26(1):36–44, 2019.

[10] Feng Shan, Junzhou Luo, Runqun Xiong, Wenjia Wu, and Jiashuo Li. Looking before crossing: An optimal algorithm to minimize uav energy by speed scheduling with a practical flight energy model.

[11] Dae Hyung Choi, Seong Hwan Kim, and Dan Keun Sung. Energy-efficient maneuvering and communication of a single uav-based relay. *IEEE Transactions on Aerospace and Electronic Systems*, 50(3):2320–2327, 2014.

[12] Uygar Demir, Merve Çiğdem İpek, Cenk Toker, and Özgür Ekici. Energy-efficient rotary-wing uav deployment under flight dynamics and qos constraints. In *2019 IEEE International Black Sea Conference on Communications and Networking (BlackSeaCom)*, pages 1–5. IEEE, 2019.

[13] Mohsen Jahanshahi and Arash Bozorgchenani. Gateway placement and selection solutions in wmns: A survey. *arXiv preprint arXiv:1906.06774*, 2019.

[14] Awadallah M Ahmed, Aisha H Abdalla, and Ismail El-Azhary. Gateway placement approaches in wireless mesh network: Study survey. In *2013 INTERNATIONAL CONFERENCE ON COMPUTING, ELECTRICAL AND ELECTRONIC ENGINEERING (ICCEEE)*, pages 545–547. IEEE, 2013.

[15] Skanda N Muthaiah and C Rosenberg. Single gateway placement in wireless mesh networks. *Proc. ISCN*, 8:4754–4759, 2008.

[16] Wenjia Wu, Junzhou Luo, and Ming Yang. Gateway placement optimization for load balancing in wireless mesh networks. In *2009 13th International Conference on Computer Supported Cooperative Work in Design*, pages 408–413. IEEE, 2009.

[17] Bassam Aoun, Raouf Boutaba, Youssef Iraqi, and Gary Kenward. Gateway placement optimization in wireless mesh networks with qos constraints. *IEEE Journal on Selected Areas in Communications*, 24(11):2127–2136, 2006.

[18] Andrea. Goldsmith. *Wireless communications*. Cambridge university press, 2005.

[19] Mcs index chart. https://www.wlanpros.com/mcs-index-charts/. Accessed: 23/06/2020.

[20] Python. https://www.python.org/. Accessed: 24/06/2020.

[21] Uav power simulator. https://github.com/rhugo97/UAV-Power-Simulator. Accessed: 24/06/2020.

[22] Numpy. https://numpy.org/. Accessed: 24/06/2020.

[23] Scipy. https://www.scipy.org/. Accessed: 25/06/2020.

[24] Sitl simulator (software in the loop) — dev documentation. https://ardupilot.org/dev/docs/sitl-simulator-software-in-the-loop.html. (Accessed on 06/20/2020).

[25] Eduardo Nuno Almeida, André Coelho, José Ruela, Rui Campos, and Manuel Ricardo. Joint traffic-aware uav placement and predictive routing for aerial networks, 2020. arXiv:2004.07371.

[26] K. Nichols and V. Jacobson. *Controlling queue delay*. Queue, vol. 10, 2012.

[27] Codel queue disc — model library. https://www.nsnam.org/docs/models/html/codel.html/. Accessed: 05/07/2020.

[28] ns-3. https://www.nsnam.org/. Accessed: 27/06/2020.

[29] Nils Aschenbruck, Raphael Ernst, Elmar Gerhards-Padilla, and Matthias Schwamborn. Bonnmotion: a mobility scenario generation and analysis tool. In *Proceedings of the 3rd international ICST conference on simulation tools and techniques*, pages 1–10, 2010.